



**HAL**  
open science

## Translocation of cell-penetrating peptides involving calcium-dependent interactions between anionic glycosaminoglycans and phosphocholine bilayer

Bingwei He, Sonia Khemaissa, Sébastien Cardon, Rodrigue Marquant, Françoise Illien, Delphine Ravault, Fabienne Burlina, Emmanuelle Sachon, Astrid Walrant, Sandrine Sagan

### ► To cite this version:

Bingwei He, Sonia Khemaissa, Sébastien Cardon, Rodrigue Marquant, Françoise Illien, et al.. Translocation of cell-penetrating peptides involving calcium-dependent interactions between anionic glycosaminoglycans and phosphocholine bilayer. Chemrxiv, 2024, 10.26434/chemrxiv-2024-6gh53 . hal-04744664

**HAL Id: hal-04744664**

**<https://hal.sorbonne-universite.fr/hal-04744664v1>**

Submitted on 19 Oct 2024

**HAL** is a multi-disciplinary open access archive for the deposit and dissemination of scientific research documents, whether they are published or not. The documents may come from teaching and research institutions in France or abroad, or from public or private research centers.

L'archive ouverte pluridisciplinaire **HAL**, est destinée au dépôt et à la diffusion de documents scientifiques de niveau recherche, publiés ou non, émanant des établissements d'enseignement et de recherche français ou étrangers, des laboratoires publics ou privés.



Distributed under a Creative Commons Attribution - NonCommercial - NoDerivatives 4.0 International License

# Translocation of cell-penetrating peptides involving calcium-dependent interactions between anionic glycosaminoglycans and phosphocholine bilayer

Bingwei He<sup>1</sup>, Sonia Khemaissa<sup>1</sup>, Sébastien Cardon<sup>1</sup>, Rodrigue Marquant<sup>1</sup>, Françoise Illien<sup>1</sup>, Delphine Ravault<sup>1</sup>, Fabienne Burlina<sup>1</sup>, Emmanuelle Sachon<sup>1,2</sup>, Astrid Walrant<sup>1</sup>, Sandrine Sagan<sup>1\*</sup>.

<sup>1</sup> Sorbonne Université, École normale supérieure, PSL University, CNRS, Laboratoire des Biomolécules (LBM), 75005 Paris, France.

<sup>2</sup> Sorbonne Université, Mass Spectrometry Sciences Sorbonne University, MS3U, platform, 75005 Paris, France.

\*Corresponding Author: Sandrine Sagan, Sorbonne Université, Laboratoire des Biomolécules, CC182, 4 place Jussieu, 75005 Paris, France.

**Email:** sandrine.sagan@sorbonne-universite.fr

ORCID: Bingwei He (0000-0002-8535-2456); Sonia Khemaissa (0009-0006-0628-2194); Sébastien Cardon; Rodrigue Marquant; Françoise Illien (0000-0003-3414-8452); Delphine Ravault (0000-0002-1849-3312); Fabienne Burlina (0000-0002-6042-680X); Emmanuelle Sachon (0000-0002-2271-8924); Astrid Walrant (0000-0003-4054-905X); Sandrine Sagan (0000-0003-0083-4411).

**Author Contributions:** A.W. and S.S. designed research; B.H., S.K., S.C., R.M., F.I., and D.R. performed research; F.B. and E.S. contributed reagents or analytic tools; B.H., S.K., A.W. and S.S. analyzed data; A.W. and S.S. wrote the paper.

**Keywords:** Translocation mechanism; cell-penetrating peptides; mini-homeoproteins; glycosaminoglycans; lipid bilayer.

**Abstract -** Cell-penetrating peptides can internalize ubiquitously in many, if not all, cell types. To explore the specific targeting issue of cell-penetrating peptides (CPPs), we studied glycosaminoglycan (GAG)-binding peptides previously identified in Otx2 and En2 homeoproteins (HPs), alone or extended with the penetratin-like third helix (H3) of En2. HPs are indeed known to internalize in specific cells, thanks to their GAG-targeting sequence (Joliot et al. 2022; Cardon et al. 2023). We quantified the capacity of these peptides to enter into various cell lines known to express different levels and types of heparan sulfates (HS) and chondroitin sulfates (CS) GAGs. We also analyzed by calorimetry (DSC, ITC) and fluorescence spectroscopy, the binary and ternary interactions between heparin (HI), (4S, 6S)CS (CS-E), zwitterionic phosphocholine (PC) model membranes and those peptides. Altogether, our results demonstrate the existence of Ca<sup>2+</sup>-dependent interactions between CS-E or HI and PC lipid bilayers, the major phospholipid found in animal cell plasma membrane. Importantly, we show that CS-E can act as a Ca<sup>2+</sup>-dependent bridge with PC membranes that can be exploited by a chimeric CS-E-recognition motif-H3 peptide to bind and cross the membrane lipid bilayer and get access directly to the cytosol of cells. Altogether, this study brings further information uncovering the molecular mechanism of the translocation process

of CPPs that implies specific GAGs at the cell-surface. It also shed light on the role of GAGs in the paracrine activity and cell specificity of HPs.

## Introduction

Cell-penetrating peptides (CPPs) are known to penetrate all cell types through two main routes concomitantly, endocytosis paths and direct translocation, the latter implying temporary and non-toxic disruption of the lipid bilayer of the plasma membrane (1). The endocytic way is quite well understood and, depending on the CPP sequence, involves almost all kinds of reported endocytosis processes (2), including atypical ones (3). By contrast, the understanding of translocation is still in its infancy, since the phenomenon is difficult to bring to light directly in cells. The decrease of temperature below 12°C (to discard endocytosis pathways), or the incubation in the presence of endocytotic inhibitors are generally used to highlight translocation in cells. Each of these two methods have their own drawbacks, since lowering the temperature impacts the fluidity and dynamics of the cell membrane, and the use of endocytotic inhibitors has side-effects that are generally overlooked (4, 5). However, we recently report with a new method that translocation of oligoarginines is similar at 37°C and 4°C (6). A recent study using the NanoBiT assay in engineered cells that expressed the LgBiT protein in the cytosol, has made one step forward in the qualification of translocation path of homeoproteins (7). One of the main results of this study was to establish the presence of the HiBiT-tagged Engrailed2 (En2) homeoprotein in the cytosol of intact cells by measuring the light emitted after its complementation with the cytosolic-expressed LgBiT protein, demonstrating the direct translocation (or endosomal escape), of the protein through the plasma membrane. Albeit the evidence for translocation, the study did not address the mechanism(s) behind, in particular the specific and required cell-membrane partners that are recruited for translocation, a process that can be assimilated as a reversible and temporary disruption of the cell membrane bilayer.

Besides, cell-surface differs from one cell type to the other in terms of the extracellular matrix content, forming a gel-like microenvironment above the lipid bilayer. The cell-surface is covered in particular by heparan sulfates (HS), and chondroitin sulfates (CS), glycosaminoglycans (GAGs), that are long anionic chains of linear and differently sulfated polysaccharides anchored on proteins (proteoglycans). Several studies reported that those GAGs are necessary for interactions with and internalization of CPPs in model systems (8) or in cells (1, 9–11). It is also well established that HS proteoglycans are involved in endocytotic pathways of different types of molecules including CPPs (12, 13). Whether HS and CS are also involved in translocation either as bystanders or active players (9, 10, 14) is therefore a question that remains to be addressed and was one objective of the present study.

CPPs are known to internalize ubiquitously in cells, this lack of cell-targeting property hampering the use of these peptides as efficient delivery tools for biotechnological or therapeutic purposes. Interestingly, it has been reported that within the sequences of En2 (15) and Otx2 (16) homeoproteins (HPs), a GAG-binding sequence upstream of the helix-3 of the homeodomain is required for the specific internalization of these proteins (15, 17) and their function in the central nervous system (16). In contrast to CPPs, HPs are indeed endowed with targeting properties towards specific regions of the brain expressing different levels and types of GAGs (18). The targeting property relies on the presence of this GAG-recognition motif upstream the homeodomain, that is the internalization or penetratin-like sequence. The GAG-targeting sequences are a pentadecapeptide, GAG<sup>Otx</sup> (RKQRRERTTFTRAQL), in Otx2 and an octadecapeptide, GAG<sup>En</sup> (RSRKPKKKNPNKEDKRPR), in En2 (Figure 1a). These peptides recognize respectively chondroitin-4,6-disulfate (CS-E) and highly sulfated HS (15, 16).

In the present study, we used four ovarian cell types that express different levels and types of HS and CS. Wild type chinese hamster ovarian cells (CHO-K1) express HS and chondroitin mono-sulfates (CS-A and CS-C); mutant GAG-deficient ovarian cells (CHO-pgsA-745) derived from K1, have genetical defects in xylosyltransferase (19) and express only 5-15% GAGs compared to K1 cells; human ovarian adenocarcinoma cells CaOV-3 overexpress HS and (4,6)-CS (CS-E), subtypes (20); finally human ovarian adenocarcinoma SKOV-3 cells overexpress CS-E (21). We

analyzed the ability of the two GAG-targeting sequences, GAG<sup>Otx</sup> and GAG<sup>En</sup>, to internalize alone into cells. We also combined these GAG-targeting peptides with the penetratin-like 3rd helix sequence of En2, H3 (SQIKIWFQNKRAKIKK), as a biomimetic approach to design mini-homeoprotein mimics retaining cell-penetration and targeting properties (Figure 1b). We examined the impact of GAGs on the internalization of all these peptides in the above-mentioned cell lines. In addition, using a combination of calorimetry (ITC, DSC), fluorescence spectroscopy and dynamic light scattering (DLS), we dissected the bi- and tripartite interactions between GAGs, phospholipids and the chimeric peptides. Our results bring evidence that CS-E is required for translocation of the CS-E targeting chimeric peptide. Of utmost interest, using model lipid systems, we show that CS-E interacts with the cationic choline headgroup of phospholipid vesicles and that this interaction depends on the presence of divalent cations, in particular Ca<sup>2+</sup>. Altogether, our results highlight the respective role and synergistic collaboration between GAGs, phosphocholine (PC) lipids and these cationic GAG targeting chimeric CPPs in the translocation pathway that leads to direct access to the cytosol of cells.

## Results

### Homeoprotein-derived GAG-binding peptides interact differently with HI and CS-E

The group of Prochiantz previously reported a motif upstream the Otx2 homeodomain that interacts preferentially with CS-E: RKQRRERTTFTRAQL (16). More recently, we identified in En2 another motif that binds highly sulfated HS, RSRKPKKKNPNKEDKRPR (15). The two motifs are not strictly aligned in the two HP sequences. We designed chimeric peptides formed by the two aforementioned GAG-recognition sequences (GAG<sup>Otx</sup> and GAG<sup>En</sup>), extended at the C-terminus by the penetratin-like H3 of En2, thus forming minimalistic homeodomain mimics (Figure 1).

Since the interaction of the GAG-recognition sequences was described in the context of HPs, we first wanted to examine whether these sequences alone still interacted with GAGs. We determined by ITC whether the designed peptides (GAG-recognition sequences alone or chimeric peptides), interact with heparin (HI) used as a mimic of highly sulfated HS, or CS-E (Table 1). The two anionic polysaccharides taken as GAG representatives differ in size, HI (12 kDa), containing about 20 disaccharides and CS-E (72 kDa), about 135 disaccharides.

HI is a highly sulfated polymer, mostly composed of trisulfated Glc(NS,6S)–IdoA(2S), which is found in *N*-sulfated domains of HS (22, 23), a key structure for protein recognition (24). In contrast, CS-E polymer is a repetition of GlcA-GalNAc(4S,6S) disaccharides.

As shown in Figure 1, all peptides, being either GAG-binding motifs or chimeric GAG-H3 sequences, are positively charged at physiological pH and can thus interact with the negatively charged polysaccharides HI and CS-E. The stoichiometry of the complexes is however weakly dependent on the peptide charge, showing that the interactions are complex and more intricate than just counter-ion electrostatics bonds (Fig. S1). The interaction (Table 1) is enthalpically-driven, indicative of H-bonds and electrostatic interactions. The formation of peptide / GAG complexes is entropically disfavored, likely because of the loss of conformational flexibility of the two interacting partners. At first glance, the favorable enthalpy, recorded during formation of the complexes, does not seem directly related to the net charge of the peptides, supporting the involvement of other types of interactions in addition to electrostatic ones (Fig. S2).

Because the stoichiometry of binding is different for each peptide, comparing  $K_d$  values derived directly from ITC experiments is not relevant (15). We thus used normalized  $K_d$  values for one peptide bound per polysaccharide unit, that were calculated using the Van't Hoff equation with the experimental  $\Delta G$ . The peptides have very different affinity for heparin, ranking from 22 mM for the highest (GAG<sup>En</sup>-H3), to 425 mM for the lowest (GAG<sup>Otx</sup>). Neither the affinity of the peptides for heparin, nor the stoichiometry of the non-covalent complex (defined as the number of peptides interacting with one HI polymer chain), seem directly linked to the net positive charge of the peptides. Besides, all peptides interact with CS-E with affinity values within the same range (510-900 mM). Altogether, these results show that GAG<sup>Otx</sup> is less selective (value of CS-E/HI affinity ratio about 2) than GAG<sup>En</sup> (value of CS-E/HI affinity ratio about 10). Interestingly, considering that

we used a HI polymer of about 20 disaccharides and CS-E of about 135 disaccharides, the results show on one side that GAG<sup>Otx</sup> binds almost every disaccharide of both heparin (17 peptides / HI chain) and CS-E (100 peptides / CS-E chain) polymer. On the other side, GAG<sup>En</sup>-H3 binds roughly 1 over 5 disaccharides in both HI and CS-E polymer chains. Interestingly, an entropy/enthalpy compensation phenomenon is observed for the formation of the peptide/GAG complexes (Fig. S3).

#### **Absence of cytotoxicity of the peptides**

The peptides were tested for their cytotoxicity in CHO-K1 cells and for hemolysis on red blood cells. Briefly, for the former assay, 5,000 CHO-K1 were incubated for 1 hr with the peptides up to 20  $\mu$ M concentration. In parallel, untreated cells were defined as positive control while the wells without cells stood as a negative control. For the latter assay, 100  $\mu$ L red blood cells solution was incubated with peptides at 10  $\mu$ M or 50  $\mu$ M for 1 hr at 37°C. As a positive control, complete cell hemolysis was obtained by incubating blood cells with 0.1% Triton X-100. The negative control was obtained by incubation of blood cells with PBS. The release of hemoglobin was measured by photometric absorption at 540 nm. In those conditions (Fig. S4), the peptides have neither cytotoxicity (up to 20  $\mu$ M) nor hemolytic activities (up to 50  $\mu$ M).

#### **GAG-binding peptides hardly internalize into cells when the internalization of chimeric peptides, is boosted in the presence of sulfate-containing GAGs**

Since all peptides interact with HI and CS-E, we wanted to next analyze their cell-penetration in cell lines expressing different levels and types of HS and CS glycosaminoglycans. Using biotin- and *N*-terminal deuterium-labeled peptides as internal standards for mass spectrometry (MS) quantification (25, 26), we evaluated, using MALDI-TOF MS, the capacity of the peptides to internalize within one-hour time incubation into different cell lines: CHO-K1, CHO-pgsA745, CaOV-3 and SKOV-3, reported to express different contents of HS and CS-E (18–20) (Fig. 2).

H3, GAG<sup>Otx</sup> and GAG<sup>En2</sup> peptides were first studied. As expected (1), the penetratin-like H3 peptide internalizes 3-times less in the pgsA 745 cell line deficient in HS and monosulfated CS, compared to K1 and SKOV-3 cells. H3 internalization is however 5-times higher in the CaOV-3 than in CHO-K1 cell line. Interestingly, the two GAG-binding peptides derived from Otx and En2 HPs, are hardly internalized (< 0.5 pmoles), in all cells, whatever their GAG content. This last result particularly emphasizes that interactions of a peptide sequence with GAGs does not necessarily lead to its internalization.

When considering chimeric peptides, the presence of GAG-recognition sequences has little effect on H3 internalization in K1 and pgsA-745. On the other hand, internalization of H3 is significantly increased (3-times) in CaOV-3 and SKOV-3 cell lines for GAG<sup>Otx</sup>-H3 but not GAG<sup>En</sup>-H3.

#### **Impact of the presence of a linker between the GAG-binding motif and the internalization H3 domain on GAG interaction, secondary structure and cell-penetration of peptides**

The first chimeric peptides were designed to connect directly the GAG-recognition and cell-penetrating peptides without any gap. To evaluate whether the GAG-binding motif and the H3 internalization domain can act at distance or under more conformational flexibility or restriction, we synthesized a series of GAG<sup>En</sup>-linker-H3 and GAG<sup>Otx</sup>-linker-H3 analogues with different linker moieties. The linker was either an aminopentanoic acid (Apa, NH<sub>2</sub>-(CH<sub>2</sub>)<sub>4</sub>-COOH), an amino-PEG<sub>2</sub>-acid (PEG<sub>2</sub>, NH<sub>2</sub>-(CH<sub>2</sub>-CH<sub>2</sub>-O)<sub>2</sub>-CH<sub>2</sub>-COOH), Pro, Gly or Gly<sub>4</sub>. It introduces a space between the GAG-binding motif and the H3 internalization domain of either conformationally constrained 3 atoms (Pro) or more flexible 3 atoms (Gly), 6 atoms (Apa), 9 atoms (PEG<sub>2</sub>) or 12 atoms (Gly<sub>4</sub>).

As seen in Fig. 3, for the GAG<sup>En</sup>-linker-H3 series, the internalization efficacy was in the best case, GAG<sup>En</sup>-Apa-H3, similar to the peptide without linker and always significantly decreased for all other analogues. In contrast, for the GAG<sup>Otx</sup>-linker-H3 series, we could obtain increased internalization for the analogue containing the longer linker (Gly<sub>4</sub>, 12 atoms), whereas the 6- and 9 atoms linker-containing analogues have similar internalization efficacy as the reference peptide without linker. Finally, the analogues containing the 3 atoms-linker (Pro, Gly), have significant decreased internalization compared to the peptide without linker. Altogether these results show that except for the Apa linker that has no influence on the internalization efficacy of the peptides, almost opposite

effects were observed with the different linkers on internalization of GAG<sup>En</sup>-linker-H3 and GAG<sup>Otx</sup>-linker-H3 analogues. This observation establishes that, depending on the GAG-recognition sequence, the chimeric peptide probably interacts with different partners or differently with the same partners at the cell-surface and consequently internalizes also differently.

The thermodynamics of these peptides interacting with HI or CS-E were therefore also studied by ITC (Table S1). Globally, formation of peptide / GAG complexes is enthalpically-driven for all peptides. Interestingly, the GAG<sup>En</sup>-linker-H3 series has higher preference for HI (ratio of  $K_d$  (CS-E) over  $K_d$  (HI) in 10-15 range), than the GAG<sup>Otx</sup>-linker-H3 series (ratio of  $K_d$  (CS-E) over  $K_d$  (HI) within 1.6-6.9 range, except for GAG<sup>Otx</sup>-Gly-H3), consistently with what was observed for the original peptides. We could not find any direct correlation however between the thermodynamics (enthalpy, stoichiometry), and the capacity of the peptide to internalize into cells.

Finally, we examined the secondary structure of the whole chimeric peptide series by CD, either alone or in interaction with HI (used at a saturating concentration previously determined by ITC), or palmitoyl-2-oleoyl-*sn*-glycero-3-phospho-rac-(1-glycerol) (POPG) vesicles. Results (Table S2), indicate that there is no structuration for all peptides in 100 mM NaF in 10 mM phosphate buffer. In the presence of HI, the GAG<sup>Otx</sup>-linker-H3 series is mostly unstructured while the addition of HI increased the peptides propensity to adopt a  $\beta$ -strand structure. In contrast, in the presence of POPG vesicles, at low peptide/lipid (P/L) ratio, the GAG<sup>Otx</sup>-linker-H3 peptides are both unstructured and  $\alpha$ -helical. With increasing P/L ratio, the preferred conformation is random coil and  $\beta$ -strand. The GAG<sup>En</sup>-linker-H3 series has no structure in 100 mM NaF, 10 mM phosphate buffer. In the presence of HI, these peptides remain principally unstructured and also populate  $\alpha$ -helix and  $\beta$ -strand conformations. In the presence of POPG vesicles, the peptides conformational preference is the random coil and slightly the  $\beta$ -strand. Altogether, these results show that these peptides are tremendously chameleon-like structures. Mostly unstructured in solution, they fit to  $\alpha$ -helices or  $\beta$ -strands depending on the interaction partner or the stoichiometry of the interaction complex.

#### **Affecting the presence and structure of GAGs at the cell-surface impairs peptide entry**

To analyze further the role of the anionic cell-surface GAGs, we next examined the effect of enzymatically- or chemically-driven alteration of SKOV-3 cell surface GAGs on peptide internalization. For that purpose, we pre-treated cells with heparinases I-III and/or chondroitinases ABC, which hydrolyze GAGs, or sodium chlorate (NaClO<sub>3</sub>), which is an inhibitor of GAG sulfatation (used at 10 and 100 mM non-cytotoxic concentrations). Results in Fig. 4 indicate that the internalization of GAG<sup>En</sup>-H3 and GAG<sup>Otx</sup>-H3 drops when the presence of sulfated GAGs is decreased. The internalization of GAG<sup>En</sup>-H3 is reduced when cells are pre-treated either by heparinases I-III (Hep I-III; 64% decrease) or chondroitinase ABC (ChABC; 40% decrease), while in the same experimental conditions, GAG<sup>Otx</sup>-H3 internalization is only affected by ChABC (38% decrease). The role of sulfatation was confirmed by treating cells with the sulfate adenylyltransferase inhibitor NaClO<sub>3</sub>. In the latter case, 10 mM NaClO<sub>3</sub> decreases by 43% GAG<sup>Otx</sup>-H3 internalization.

Altogether, the effect of NaClO<sub>3</sub> and enzymatically-driven degradation of cell-surface GAGs on peptide internalization is not surprising, since a constitutive clathrin- and caveolin-independent endocytic pathway (27), is involved in the internalization of heparan sulfate proteoglycans (HSPGs) and HSPG-binding molecules essential for cell maintenance and signaling (28, 29).

Whether GAGs can also directly interact with the cell membrane lipid bilayer and be involved in direct membrane crossing of peptides by a translocation process has not been well documented so far. Since a few decades, it is however known that efficient extraction of plasma HI includes a stringent delipidation step (30). Concomitant with this latter observation, phosphocholine is found as the major plasma HI binding lipid. Therefore, we next addressed whether HI and phospholipids can interact together.

#### **Calcium-dependent interactions of HI and phosphocholine (PC) in model membranes**

Since the major phospholipids of the animal cell membrane lipid bilayer contain the phosphocholine headgroup, we used (14:0)PC (1,2-dimyristoyl-*sn*-glycero-3-phosphocholine, DMPC), large unilamellar vesicles (LUVs), to test by DSC whether HI could modify the thermotropic phase

behavior of this phospholipid (Fig. 5). The pre-transition peak of 1,2-dimyristoyl-*sn*-glycero-3-phosphocholine (DMPC), appears around 15°C, while the main transition is recorded at 25°C along with an associated enthalpy about 20 kJ.mol<sup>-1</sup>.

Addition of increasing amounts of HI in the presence of divalent cations (Mg<sup>2+</sup>, Ca<sup>2+</sup>), leads to the gradual increase of the pre-transition and main-transition temperatures, together with an increase of the area of the main phase transition peak (Fig. 5b). By contrast, there is no change in the pre-transition and main transition peaks in the absence of Ca<sup>2+</sup>, Mg<sup>2+</sup> even at the maximal ratio (1/100) of HI/DMPC (Fig. 5a), consistently with reports from the literature (31). The corresponding thermodynamic parameters  $\Delta H$  and  $T_m$  for the different HI/DMPC ratios in the absence (a), or the presence of Ca<sup>2+</sup>, Mg<sup>2+</sup> (b), are shown in Fig. 5c and 5d. These results indicate that HI interacts with the head group of DMPC in the presence of the divalent cations, compresses phospholipids and leads to reduced hydrophobic forces between alkyl chains. The interaction between alkyl chains of DMPC requires more energy to shift from gel state to fluid phase so that  $T_m$  reached 26°C (Fig. 5c) at the highest HI/DMPC ratio. A similar trend is observed with the phospholipids dipalmitoylphosphatidylcholine (DPPC or (16:0)PC), and distearoylphosphatidylcholine (DSPC or (18:0)PC) (Fig. S5). In the presence of increasing amounts of HI with DPPC LUVs, the pre-transition peak becomes wider before disappearing and  $T_m$  shifts to higher temperature (Fig. S5). For DSPC, the pre-transition becomes invisible and the main transition peak is broadened and likely splits into HI-rich (wider) and HI-poor (sharper) regions. For the two phospholipids, the enthalpy increases, showing that HI induces phospholipid compression. These results confirm that a polyanionic GAG can interact with the phosphocholine lipid bilayer found in the animal cell plasma membrane.

### **Ternary interactions between GAGs, PC vesicles and peptides**

We questioned next whether these interactions between GAGs and PC lipid bilayers would be affected by the chimeric peptides, GAG<sup>Otx</sup>-H3 or GAG<sup>En</sup>-H3. We prepared DMPC LUVs decorated with either HI at a ratio of 1/500 or CS-E at a ratio of 1/1000. The positively-charged peptides hardly interact with LUVs of DMPC as previously reported (32) but affect the DMPC main transition in the presence of GAGs (Fig. 6a, b, d, e). The trend is different for HI versus CS-E-decorated LUVs, but quite similar for the two chimeric peptides. The relative  $\Delta H$  curves (Fig. 6c, f) of DMPC and HI-decorated DMPC LUVs rapidly converge upon the first addition of peptide (ratio = 0.01).

In contrast, GAG<sup>En</sup>-H3 increases the enthalpy at 0.01 peptide/HI-DMPC ratio before overlaying the DMPC curve afterwards. This observation is emphasized in the case of GAG<sup>Otx</sup>-H3. With this latter peptide, the enthalpy is increased for the peptide/LUV ratio between 0.01 and 0.04, consistent with the simple adsorption of the peptide at the surface of CS-E-decorated vesicles that results in lipid ordering. At a certain peptide/vesicle threshold (>0.04), the trend reverses with a decrease of enthalpy to reach a value slightly lower than the one measured for LUVs alone (Fig. 6). This observation likely reflects insertion of the peptide between the acyl chains of DMPC.

Altogether, these results indicate that GAG<sup>Otx</sup>-H3 and to a lesser extent GAG<sup>En</sup>-H3, can interact with DMPC lipid bilayers covered by anionic GAGs in the presence of calcium divalent cation, more particularly CS-E in the context of this study.

### **GAG<sup>Otx</sup>-H3 intercalates into PC membranes in the presence of Ca<sup>2+</sup>-dependent CS-E-bridge**

In the above experiments, we evidenced the existence of ternary interactions between anionic GAGs, zwitterionic PC lipid bilayers and the chimeric peptides. We propose that CS-E could directly interact with the cell membrane and establish a bridge for peptide interaction with the lipid bilayer of the plasma cell membrane. We further tested this hypothesis by monitoring Trp fluorescence in peptides interacting with model membranes that mimic the cell one, as the two chimeric peptides contain one Trp residue in the common H3 segment of their sequence. We analyzed the partitioning of the two peptides within PC LUVs either alone or decorated at their surface by HI or CS-E, as well as their interaction with GAGs, in the absence of lipids, considering that binding to a GAG

could possibly lead to a change in the Trp environment and thus be accompanied by a shift of the maximum emission wavelength.

As expected, Trp fluorescence intensity increases linearly according to the peptide concentration (Fig. S7). Upon addition of increasing concentrations of DOPC LUVs (Fig. S8), no shift of Trp wavelength emission ( $\lambda_{em}$ ) is observed, indicating the absence of modification of the Trp environment, thus reflecting the absence of partitioning of the peptides into PC vesicles in these conditions. By contrast, addition of HI- or CS-E-decorated DOPC LUVs shifted  $\lambda_{max}$  to lower wavelengths (Table 2).

This blue shift, indicative of a more hydrophobic environment of the Trp residue, increased to a maximum of 14-18 nm when GAG<sup>En</sup>-H3 binds HI or HI-decorated PC vesicles, with an apparent affinity  $K_d^{app}$  in the  $\mu$ M range similar in the two cases. In the case of CS-E and CS-E-decorated vesicles, the  $\lambda_{max}$  is shifted by 6-7 nm and the affinity of GAG<sup>En</sup>-H3 is within the same range for CS-E-decorated vesicles than for CS-E alone, respectively 440 nM and 250 nM. In any case, it appears that GAG<sup>En</sup>-H3 only interacts with the GAG and does not insert into the PC membrane.

GAG<sup>Otx</sup>-H3 shows a very different behavior in the binding to CS-E and CS-E decorated vesicles (Fig. S9, Table 2). In both cases, the blue shift increases up to 14 nm but GAG<sup>Otx</sup>-H3 has a significantly 4-times higher affinity for CS-E-decorated vesicles (130 nM), than for CS-E alone (500 nM). This observation does not result from disruption/destruction of the vesicles since no calcein leakage could be observed in parallel under the same experimental conditions (Fig. S10). Interestingly, the binding parameters for CS-E-decorated vesicles and POPG vesicles are in the same range (Fig. S9, Table 2). In addition, in the absence of Ca<sup>2+</sup>, the affinity of GAG<sup>Otx</sup>-H3 is in the range of 500 nM both for CS-E or CS-E-decorated DOPC. Altogether, these results strongly support a partitioning of the peptide into DOPC lipid bilayers, only in the presence of CS-E and calcium. Finally, the peptide has similar binding parameters to HI or HI-decorated PC vesicles.

Altogether, these results evidence that in the presence of Ca<sup>2+</sup>, CS-E-decorated PC vesicles can mimic negatively charged phospholipid bilayers that cationic peptides are known to insert into. These properties are not shared by HI which was used herein as a HS mimic. These results also highlight the difference of behavior between GAG<sup>En</sup>-H3 and GAG<sup>Otx</sup>-H3. In the conditions used herein, the chimeric peptide GAG<sup>En</sup>-H3 has no discriminating ability to bind to PC lipid bilayers in the presence of GAGs. On the contrary, GAG<sup>Otx</sup>-H3 has the selective ability to bind CS-E-decorated PC vesicles and, in the presence of the GAG, to insert between the alkyl chains of the PC lipid bilayer. CS-E lying on top of PC might be assimilated therefore as a "polar negatively charged headgroup" in CS-E-decorated DOPC vesicles. This observation supports the involvement of CS-E and calcium interactions with the lipid bilayer of cells for GAG<sup>Otx</sup>-H3 translocation mechanism.

### **CS-E improves selectively translocation of GAG<sup>Otx</sup>-H3 in cells**

To study whether these ternary interactions may also occur in cells and impact the internalization of the peptides, in particular the translocation process supported by results from the lipid model systems from the previous section, we analyzed the effect of exogenous HI or CS-E on the internalization efficacy of the chimeric peptides. We first worked with pgsA-745 CHO cells lacking HS and CS (19), and as a mimic of GAG-decorated PC vesicles, we incubated GAG-deficient cells with a mixture of HI or CS-E and the chimeric peptides.

As shown in Fig. 7a, incubation of GAG-deficient cells with each of the peptides in the presence of increasing HI concentrations boosts the quantity of their internalization. At the maximal concentration tested (7.2  $\mu$ g/mL HI), about 20 pmol of GAG<sup>En</sup>-H3 and 30 pmol of GAG<sup>Otx</sup>-H3 is internalized after 1hr incubation with cells. The situation is very different with CS-E (Fig. 7b). On the one side, addition of increasing concentrations of exogenous CS-E does not modify the quantity of GAG<sup>En</sup>-H3 internalized within 1hr incubation with cells. On the other side, the addition of exogenous CS-E significantly boosts the quantity of internalized GAG<sup>Otx</sup>-H3. At the maximal concentration tested (7.2  $\mu$ g/mL CS-E), the quantity of GAG<sup>Otx</sup>-H3 inside cells is roughly 5-times greater than in the absence of CS-E.

To understand the processes behind these observations, we determined in parallel the size (obtained from dynamic light scattering experiments), and charge surface (measured through determination of the zeta potential), of the peptide/GAG complexes (Fig. S11). No major difference

in the size of the complexes is measured at the highest concentrations of HI or CS-E. The size of HI/GAG<sup>En</sup>-H3 and CS-E/GAG<sup>En</sup>-H3 complexes is about 150 and 170 nm, respectively. The size of HI/GAG<sup>Otx</sup>-H3 and CS-E/GAG<sup>Otx</sup>-H3 complexes is about 260 and 170 nm, respectively. All complexes have a positive zeta potential.

Therefore, the size and charge of all GAG/peptide complexes are not different from each other and cannot explain the difference observed in peptide internalization in the presence of exogenous GAGs. One plausible explanation is that HI/peptide complexes can internalize by endocytosis into GAG-deficient cells while CS-E could selectively improve direct translocation of GAG<sup>Otx</sup>-H3 only.

To improve further this hypothesis, we used CaOV-3 cells for which an overexpression of both HS and CS-E has been reported (20). In these cells, exogenous HI still improves the internalization of GAG<sup>En</sup>-H3 (Fig. 7c), while addition of exogenous CS-E decreases the quantity of GAG<sup>Otx</sup>-H3 in cells (Fig. 7d). These data indicate that endocytosis route for HI/GAG<sup>En</sup>-H3 complexes is active, although reduced (2- to 3-folds compared to GAG-deficient cells, not shown), with limited competition with cell-surface endocytosis-supporting GAGs. By contrast, GAG<sup>Otx</sup>-H3 internalization is significantly slightly decreased in the presence of CS-E, suggesting that the exogenously added CS-E competes with the cell-surface CS-E to interact with the peptide. At 7.2 µg/mL CS-E this competition no longer occurs. These results strongly suggest that the exogenous CS-E first cannot interact with the lipid bilayer, likely because the CS-E expressed at the cell-surface already covers the lipid bilayer. These results reinforce the idea that the cell-surface CS-E can form a bridge that allows the specific-recognition by GAG<sup>Otx</sup>-H3 peptide, promoting its interaction with the lipid bilayer and its translocation across the plasma membrane of the cells.

## Discussion

With this study, we bring further clues for the complex mechanism of internalization of CPPs derived from HPs. CPPs are known to internalize ubiquitously in any cell type, which is a major drawback for their applications in therapeutics or diagnostics. We and others recently identified within HPs, GAG-targeting sequences upstream the penetrating H3 domain (15, 16). We have characterized herein the potency of these sequences to endow CPPs with cell-targeting properties. In addition, we moved one step forward in the mechanism of internalization involving GAGs at the cell-surface. CPPs enter cells through two major pathways, endocytosis and translocation. Depending on their amino acid content and sequence, these peptides, often cationic and containing hydrophobic residues, can indeed interact with various partners at the cell-surface which are differently competent for internalization (1, 8-11, 33, 34).

Whatever their route of internalization, these peptides first meet the glycocalyx surrounding cells. The major components of the glycocalyx are HS and CS GAGs and the thickness of the glycocalyx might be 50 to 100 times larger than that of the cell membrane phospholipid bilayer (35). HS and CS that are ubiquitously present in proteoglycans, are long linear and hydrophilic polymers of hundreds to thousands of disaccharide units that carry strong negative charge thanks to the presence of sulfate groups. HS and CS vary from one cell type to the other in terms of sulfation level and position.

Our results indicate that GAGs are important promoters for peptide internalization in cells, but also that GAG-recognition is not sufficient to penetrate inside cells. The GAG-targeting sequences are indeed hardly internalized into cells compared to the cell-penetrating peptide derived from the third helix of En2 HP. Interestingly, the chimeric peptides combining the GAG-recognition and the cell-penetration motifs have internalization efficacy modulated by the type of GAGs present at the cell-surface. The use of heparinases or chondroitinases confirms the role of GAGs in the internalization of both GAG<sup>En</sup>-H3 and GAG<sup>Otx</sup>-H3. However, the identification of the relative contribution of HS and CS in the mechanisms of entry of the peptides is biased by the impossibility to prove the partial or total removal from the cell surface of the GAGs specifically targeted by these enzymes. To reinforce the role of GAGs, the use of sodium chlorate, which prevents the incorporation of sulfates during

GAG biosynthesis, confirms the implication of the sulfated polysaccharides in the internalization process.

Regarding the internalization pathways, GAGs are already known to be involved in constitutive clathrin- and caveolin-independent endocytic pathway (27), and HSPGs are primary receptors for many ligands essential for cell signaling (28, 29).

Apart from these endocytosis pathways, it has been demonstrated *in vitro* that HI can interact with PC. Interestingly, this interaction, most likely between the quaternary ammonium group of the polar head group of the phospholipid and the sulfate group of the GAG, switches the physico-chemical properties of HI. HI is indeed insoluble (98.5%) in chloroform while in interaction with PC, HI becomes essentially soluble (74%) in this solvent (30).

In addition, it has been reported that in the presence of  $\text{Ca}^{2+}$ , the anionic phosphate group is far enough from the cationic polar head of PC, and deeply embedded in the bilayer (36).  $\text{Ca}^{2+}$  likely acts as a counter-ion of the negatively charged phosphate groups of PC lipids found in the membrane bilayer. When calcium ions are removed, the quaternary ammonium headgroup of the phospholipid likely reorients to interact with the phosphate, and is no longer available for interactions with endogenous GAGs. In this situation, the steric hindrance and charge repulsion between adjacent phospholipids likely lead to repulsion between phospholipids and to loose bilayers.

In addition, other studies have brought evidence that the same type of interaction occurs between CS and PC in the presence of  $\text{Ca}^{2+}$  (37–39). Interestingly, Satoh and collaborators found in particular that CS chains of proteoglycans adhere to the surface of the PC membrane while HS chains stretch outward from the membrane surface. Moreover, CS contributes to the formation of PC microdomains in the outer leaflet of the cell membrane (38).

In our study, we also showed in model systems that both HI and CS-E can interact with PC, only in the presence of  $\text{Ca}^{2+}$ . However, only the chimeric peptide targeting CS-E (GAG<sup>Otx</sup>-H3) was able to insert between the alkyl chains of CS-E decorated PC vesicles and showed increased translocation in GAG-deficient cells in the presence of exogenous CS-E. This process does not lead to the formation of permanent and big holes within the bilayer, since no calcein leakage is observed in parallel. In agreement, when we used CS-E enriched CaOV-3 cells, exogenous CS-E competed with cell-surface ones and prevented GAG<sup>Otx</sup>-H3 entry through translocation. By contrast, in the presence of HI, both chimeric peptides show enhanced internalization in GAG-deficient cells, occurring through endocytotic processes of HI/peptide complexes (Fig. 8).

GAGs at the cell-surface have specific location and topology. CS that are closer to the lipid bilayer, can interact with the choline headgroup of the lipid bilayer and spread out on the cell-surface. On their side, HS stretch outward the cell-surface. We may assume that cationic peptides first meet HS at the cell-surface. Peptides with a CS-recognition motif can then transfer to CS to interact finally with the lipid bilayer, intercalate within the acyl chains and translocate within the cytosol. One plausible hypothesis to explain this transfer, which implies binding from a negatively charged polysaccharide to another, relies on the difference of binding kinetics between solution and membrane-bound partners. Huang et al. have recently reported that interaction with supported-partners can be one order of magnitude faster than with partners in solution (40). The faster kinetics of peptide binding with membrane-supported versus solution GAGs could thus arise from an increase in the encounter rate of 2D versus 3D search. The magnitude of the phenomenon totally depends on the cell size, and is likely to be 20-30 folds faster for the 10-20  $\mu\text{m}$  cells used in this study (40). Altogether, this study highlights the possibility to endow CPPs with cell specific entry (Fig. 8), and importantly likely through GAG-assisted translocation, by adding a peptide motif that specifically recognizes a CS motif bound at the cell-surface. This finding opens new perspectives for the development of therapeutical or biotechnological applications using CPPs, as well as for the elucidation of the role of GAGs in the paracrine activity and cell specificity of HPs.

## Materials and Methods

### Materials

Standard tert-butyloxycarbonyl (Boc) protected L-amino acids, 4-Methylbenzhydramine Resin (0.54 mmol/g) and 2-(1H-Benzotriazol-1-yl)-1,1,3,3-tetramethyluronium hexafluorophosphate (HBTU), Hexahydro-2-oxo-1H-thieno[3,4-d]imidazole-4-pentanoic acid (D-Biotin) were purchased from IRIS Biotech GmbH (Marktredwitz, Germany), Glycine-*N*-t-BOC (2,2-D<sub>2</sub>, 98%) was obtained from Cambridge Isotope Laboratories (Andover, MA). Dimethylformamide (DMF), Trifluoroacetic acid (TFA), Dichloromethane (DCM), diisopropylethylamine (DIEA), acetonitrile (ACN), and piperidine were obtained from Carlo Erba (France). Hydrofluoric acid (HF) was obtained from GHC Gerling Holz & Co. (Germany) and was installed in an HF Teflon apparatus (Toho, Japan). 5-(Boc-amino)pentanoic acid (Apa) and 5-Carboxy-fluorescein (FAM) were obtained from BaChem (Switzerland). Anisole, dimethyl-sulfide,  $\alpha$ -cyano-4-hydroxycinnamic acid (CHCA), Heparinase I, Heparinase II, Heparinase III, Chondroitinase ABC and Dioleoyl phosphatidylcholine (DOPC) were bought from Sigma–Aldrich (US). Streptavidin-coated magnetic beads (Dynabead® M-280 Streptavidin or Dynabead® MyOne Streptavidin C1) were bought from Invitrogen. 1-Palmitoyl-2-oleoyl-*sn*-glycero-3-phosphocholine (POPC) was purchased from Avanti Polar Lipids (USA). Phospholipids 1,2-dimyristoyl-*sn*-glycero-3-phosphocholine (DMPC), 1,2-dipalmitoyl-*sn*-glycero-3-phosphocholine (DPPC), 1,2-distearoyl-*sn*-glycero-3-phosphocholine (DSPC), and 1-palmitoyl-2-oleoyl-*sn*-glycero-3-phospho-(1'-rac-glycerol) (sodium salt, POPG), were purchased from Genzyme (Switzerland). Cell-counting kit-8 (CCK-8) was obtained from Dojindo Laboratories (Japan).

### Peptide synthesis

The peptides H3, GAGs-binding motifs GAG<sup>Ox</sup> and GAG<sup>En</sup> were assembled on a 0.2 millimolar scale by using the stepwise tBoc solid-phase synthesis strategy using HBTU as a coupling reagent. After synthesis of the peptide sequences, the peptides on resin were divided into three groups, two of which were respectively elongated by either four non-deuterated (H-peptide) or four deuterated (<sup>2</sup>H-peptide) glycine residues followed by addition of biotin. Biotinylated [<sup>1</sup>H]peptides and [<sup>2</sup>H]peptides were cleaved from the resin by treatment with anhydrous HF (2 h, 0°C) in the presence of scavenger anisole (1.5 mL/g peptidyl resin) and dimethyl sulfide (0.25 mL/g peptidyl resin). Cleaved peptides were precipitated in diethyl ether and then dissolved in 10% acetic acid. The crude peptides were lyophilized and further purified by preparative reverse-phase HPLC on a C18 column with a linear increasing acetonitrile (ACN) gradient in an aqueous solution containing 0.1% (v/v) TFA. The purity of peptide was more than 95% according to the analytical HPLC evaluation. 1  $\mu$ L purified peptide solution was mixed with 1  $\mu$ L 10 mg/mL CHCA matrix and subsequently verified by MALDI-TOF mass spectrometry (Voyager DE-PRO, Applied Biosystems). Chimeric peptides GAG<sup>Ox</sup>-H3 and GAG<sup>En</sup>-H3 were obtained from the peptide synthesis facility (Christophe Piesse, Sorbonne université, Paris, France; <https://www.ibps.sorbonne-universite.fr/en/core-facilities/pe/peptide-synthesis>).

### Liposome preparation

Phospholipids were dissolved into chloroform for the preparation of 1mg/mL large unilamellar vesicles (LUVs). Chloroform was evaporated by slow N<sub>2</sub> flow with quick rotation to prepare a homogenous lipid white film on the glass tube wall. The rest of chloroform was further removed completely in a vacuum chamber for 2 hrs. Films were then hydrated by the addition of 1mL 10 mM HEPES buffer containing 150 mM NaCl, 2 mM CaCl<sub>2</sub>, 1 mM MgCl<sub>2</sub> and mix strongly under vortex for 10 s to complete the dissolution of lipid films. The obtained multi-lamellar vesicles (MLVs) were then subjected to five freeze-thawing cycles at a temperature above the main transition temperature. Then LUVs are collected after 15-times extrusion of the homogenous lipid suspension filtered through a 100 nm Nuclepore™ track-etch polycarbonate membrane (Whatman, UK) by a mini extruder (Avanti Lipids, Alabaster, AL) at a temperature above the T<sub>m</sub> of the lipids.

### **Isothermal titration calorimetry (ITC)**

ITC experiments were performed at 25°C with a nano-ITC microcalorimeter (TA Instruments, New Castle, DE, USA). Peptides and GAGs were prepared in 10 mM HEPES containing 150 mM NaCl, 2 mM CaCl<sub>2</sub> and 1 mM MgCl<sub>2</sub> (pH=7.4). 10 µL aliquots of polysaccharides (HI or CS-E) solution were automatically injected into the 1 mL cell chamber containing peptide or lipids solution at intervals of 5 min and 250 rpm stirring speed. Peptides and polysaccharide solutions were used at different concentrations relying on the peptide sequence and GAG species (varying between 15 and 80 µM for peptides, 15 and 80 µM for polysaccharides). Equivalent HI or CS-E alone was injected into the HEPES buffer for baseline correction. Control experiments were recorded to evaluate the dilution heat of injected solution in buffer solution alone. Experimental raw data were integrated as the amount of heat generated per second during titration and fitted to a theoretical single-binding site titration curve. The thermodynamic parameters dissociation constant ( $K_D$ ), enthalpy change ( $\Delta H$ ), entropy change ( $\Delta S$ ) and stoichiometry ( $n$ ) of reaction were subsequently determined by NanoAnalyze software provided by TA Instruments. Experiments were repeated at least 2 times independently.

### **Differential scanning calorimetry (DSC)**

DSC experiments were performed with a high-sensitivity calorimeter (TA Instruments) through spectra of successive heating and cooling scans (1°C/min) of 300 µl of 1 mg/mL liposomes. Nine scans were obtained for each set and each scanning spectrum should be basically identical. There was a 10-min interval between each scan to allow thermal equilibration. Peptides or GAGs are added stepwise to liposomes to obtain peptides/lipids molar ratios of 1/100, 1/50, 1/25 and 1/10 or GAGs/lipids molar ratios of 1/1000, 1/500, 1/200, 1/100 in each set of scans. The scan of HEPES was conducted as blank for baseline correction. Parameters of pre-transition temperature (pre- $T_m$ ), main transition temperature ( $T_m$ ) and heat capacity change  $\Delta H$  (the main transition peak area) were analyzed by the fitting program NanoAnalyze provided by TA Instruments. Five to six heating and cooling scans in each set were performed.

### **Dynamic Light Scattering (DLS) measurements**

The size and zeta ( $\zeta$ ) potential of the peptide/GAG complexes was determined by DLS. Peptide and GAGs were mixed at the indicated concentrations, that is one peptide and GAGs (HI or CS-E), were added to 250 µl MQ water to form final 7.5 µM peptide and 1.8 µg/ml or 7.2 µg/ml GAG. Hydrodynamic diameters and  $\zeta$ -potential of the complexes were measured by using a Zetasizer Nano ZS apparatus (Malvern Instruments, United Kingdom).

### **Trp fluorescence measurements**

Tryptophan (Trp) fluorescence emission spectra were monitored by a fluorometer mentioned above. The excitation wavelength of Trp is 280 nm and the corresponding spectra from 300 and 420 nm are recorded. Acquisition duration of 0.5 sec/1 nm twice was conducted. Concentrations of 10, 20, 30, 40, 50 µM peptides were prepared in 100 µL 10 mM HEPES buffer (150 mM NaCl, 2 mM CaCl<sub>2</sub> and 1 mM MgCl<sub>2</sub>, pH 7.4) and their fluorescence intensity was measured as a standard peptide dilution curve. 20 µM peptide was titrated by stepwise addition of 10 µM CS-E or 80 µM HI in HEPES buffer. The fluorescence intensity of each titration was corrected by taking into account the peptide dilution. Raw spectra were smoothed by Prism GraphPad (10 neighbor points), the fluorescence intensity and maximal emission wavelength were subsequently obtained. The nonlinear titration fit was plotted by the maximal emission wavelength change  $\Delta\lambda_{max}$  according to the corresponding GAG concentration. The  $K_D^{app}$  was determined with Prism one site-specific binding. For GAG modified LUVs, firstly 40 mM DOPC LUVs (or POPG LUVs) and 10 mM DOPC LUVs were prepared in HEPES buffer, then 80 µM HI was added to 40 mM DOPC LUVs (1/500) or 10 µM CS-E was added to 10 mM DOPC LUVs (1/1000) for 15 min incubation at room temperature to form GAG modified LUVs. Finally, 20 µM GAG<sup>En</sup>-H3 and GAG<sup>Otx</sup>-H3 were titrated by GAGs-decorated LUVs respectively and the spectra were analyzed as described above. GAG<sup>Otx</sup>-H3 was also titrated by CS-E and CSE-decorated DOPC in 10 mM HEPES buffer

containing 150 mM NaCl without Ca<sup>2+</sup> or Mg<sup>2+</sup>. The experiment was repeated independently at least two times.

### **Cell culture**

Wild type Chinese Hamster Ovary (CHO-K1) cells and GAGs-deficient mutant CHO-745 cells which lack the xylosyltransferase needed for glycosaminoglycan (GAG) synthesis were grown in Dulbecco's modified Eagle's medium F-12 (DMEMF-12) with L-glutamine and 15 mM HEPES. HEK cells and HeLa cells were grown in DMEM with 4.5 g/L D-glucose and pyruvate. Two types of human ovarian cancer cell lines CaOV-3 and SKOV-3 were cultured in DMEM with Glutamax and McCoy's 5A medium respectively. All complete culture medium was supplemented with 10% fetal bovine serum, penicillin (100,000 IU/L), streptomycin (100 mg/L). Cells were grown in a humidified atmosphere at 37 °C and 5% CO<sub>2</sub>.

### **Cell treatments**

Cells need to be treated before peptide incubation. For GAGs desulfation, sodium chlorate was added to the medium to obtain 10 µM or 100 µM concentrations along with SKOV-3 cells seeding on a 12-well plate for 24 hrs. Cells were then incubated with peptides (7.5 µM) for 1 hr. As for GAGs degradation, 500 µL 2 U/mL chondroitinase ABC (ChABC) or Heparinase I II III in Tris buffer (50 mM Tris, 60 mM sodium acetate trihydrate, 0.02% BSA, pH 8) are prepared and incubated with cells for 2 hrs at 37°C, then cells are gently washed with HBSS for three times. Peptides in 500 µL DMEM were incubated with cells and treated immediately with supplementation of exogenous GAGs for 1 hr incubation. Exogenous HI fragments were obtained by heparinases pretreatment 10 min at 37°C and then were added to the cells with peptides together.

### **Quantification peptide cellular uptake by MALDI-TOF MS**

Cellular uptake was quantified by matrix-assisted laser desorption ionization time-of-flight mass spectrometry (MALDI-TOF MS) protocol. Briefly, this protocol requires isotope-labeled (deuterated glycines are present as a spacer between the peptide sequence and the *N*-terminal biotin) and unlabeled peptides: biotiny-[<sup>1</sup>H]G<sub>4</sub>-peptide, biotiny-[<sup>2</sup>H]G<sub>4</sub>-peptide. Biotin was used to capture peptides in cell lysate with streptavidin-coated magnetic beads. The deuterated peptides were used as internal standard for the absolute measurement of internalized non-deuterated peptides. 10<sup>6</sup> cells per well, seeded 24 h before the experiment in 12-well plates, were incubated with the biotiny-[<sup>1</sup>H]G<sub>4</sub>peptide (7.5 µM) in serum-free DMEM F-12 medium for 60 min at 37°C. After incubation and washes, the remaining membrane-bound <sup>1</sup>H-peptides were hydrolyzed by trypsin (37°C). 100 µL 5 mg/mL soybean trypsin inhibitor (Calbiochem) and 1 mg/mL bovine serum albumin (BSA) was added to stop digestion. The cells were then washed by 1 mL 50 mM Tris buffer containing 0.1mg/mL BSA and lysed in 150 µL lysis buffer containing 0.3% Triton, 1M NaCl, pH 7.4 and a known amount of the biotiny-[<sup>2</sup>H]G<sub>4</sub>-peptide. The cell lysate is then immediately boiled at 100°C for 15 min. The cell lysate is then incubated with C1 streptavidin-coated magnetic beads for 75 min to capture both non-deuterated and deuterated peptides. Peptides are eluted from the streptavidin-coated magnetic beads by addition of CHCA matrix(acidic pH) and spotted on the MALDI plate. Samples are analyzed in positive ion mode with MALDI-TOF on a Voyager-DE Pro mass spectrometer (Applied Biosystems, Foster City, CA, USA) in linear mode (chimeric peptides) or reflector mode (En2H3, GAG-binding peptides). For the linear mode, the MS parameters were optimized as: Accelerating voltage 25000 V; Grid voltage: 95%; Extraction delay time: 350 nsec. The absolute quantities of peptide were calculated through the ratio of the peaks areas corresponding to the non-deuterated peptides and deuterated peptides. The ratio of peaks areas was determined via Data Explorer and the quantification software we developed [15]. To be accurate, the quantification of cellular internalization requires working with an identical number of cells under different experimental conditions. For every experiment, we performed triplicate wells. The molecular weight of three chimeric peptides being high, reflector mode was not appropriate since peptides were not detected. Therefore, linear mode which is a low-resolution mode was required. Quantification was possible using a deconvolution free software recently developed [15].

## Acknowledgments

The authors thank the MS3U facility for valuable assistance with MS quantification. Research reported in this publication was supported by the Agence Nationale de la Recherche (ANR) under award number ANR-20-CE44-0018 and by the Chinese Scientific Council (CSC) PhD grant for B.H.

## References

1. Jiao CY, et al. (2009) Translocation and endocytosis for cell-penetrating peptide internalization. *J Biol Chem* 284(49):33957–33965.
2. Ruseska I, Zimmer A (2020) Internalization mechanisms of cell-penetrating peptides. *Beilstein J Nanotechnol* 11:101–123.
3. Trofimenko E, Homma Y, Fukuda M, Widmann C (2021) The endocytic pathway taken by cationic substances requires Rab14 but not Rab5 and Rab7. *Cell Rep* 37(5):109945.
4. Ivanov AI (2008) Pharmacological inhibition of endocytic pathways: Is it specific enough to be useful? *Methods Mol Biol* 440:15–33.
5. Vercauteren D, et al. (2010) The use of inhibitors to study endocytic pathways of gene carriers: optimization and pitfalls. *Mol Ther* 18(3):561–569.
6. Amblard I, et al. (2020) Bidirectional transfer of homeoprotein EN2 across the plasma membrane requires PIP2. *J Cell Sci* 133(13). doi:10.1242/jcs.244327.
7. Illien F, Bánóczy Z, Sagan S (2024) A Quantitative Method to Distinguish Cytosolic from Endosome-Trapped Cell-Penetrating Peptides. *ChemBioChem* e202400198. doi:10.1002/cbic.202400198.
8. Pae J, et al. (2016) Glycosaminoglycans are required for translocation of amphipathic cell-penetrating peptides across membranes. *Biochim Biophys Acta - Biomembr* 1858(8):1860–1867.
9. Bechara C, et al. (2013) Tryptophan within basic peptide sequences triggers glycosaminoglycan- dependent endocytosis. *FASEB J* 27(2):738–749.
10. Bechara C, et al. (2015) Massive glycosaminoglycan-dependent entry of Trp-containing cell-penetrating peptides induced by exogenous sphingomyelinase or cholesterol depletion. *Cell Mol Life Sci* 72(4):809–820.
11. Takechi-Haraya Y, et al. (2017) Glycosaminoglycan Binding and Non-Endocytic Membrane Translocation of Cell-Permeable Octaarginine Monitored by Real-Time In-Cell NMR Spectroscopy. *Pharmaceuticals* 10(4):42.
12. Christianson HC, Belting M (2014) Heparan sulfate proteoglycan as a cell-surface endocytosis receptor. *Matrix Biol* 35:51–55.
13. Mandarini E, et al. (2020) Endocytosis and trafficking of heparan sulfate proteoglycans in triple-negative breast cancer cells unraveled with a polycationic peptide. *Int J Mol Sci* 21(21):1–13.
14. Favretto ME, Wallbrecher R, Schmidt S, van de Putte R, Brock R (2014)

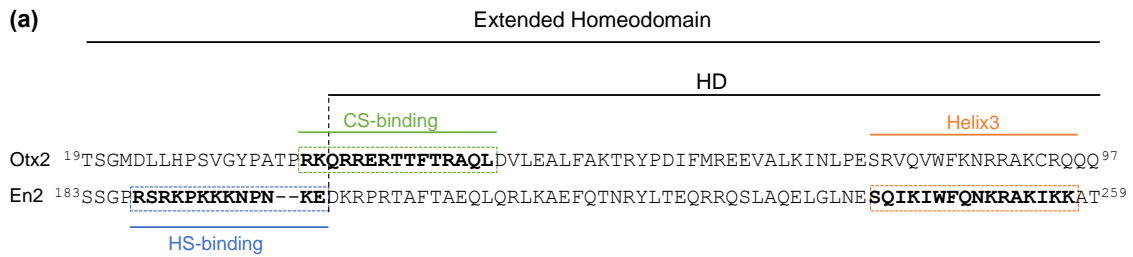
Glycosaminoglycans in the cellular uptake of drug delivery vectors – Bystanders or active players? *J Control Release* 180(1):81–90.

15. Cardon S, et al. (2023) A cationic motif upstream Engrailed2 homeodomain controls cell internalization through selective interaction with heparan sulfates. *Nat Commun* 14(1):2021.07.29.454375.
16. Beurdeley M, et al. (2012) Otx2 binding to perineuronal nets persistently regulates plasticity in the mature visual cortex. *J Neurosci* 32(27):9429–9437.
17. Joliot A, Prochiantz A (2022) Unconventional Secretion, Gate to Homeoprotein Intercellular Transfer. *Front Cell Dev Biol* 10(June):1–9.
18. Di Nardo AA, Fuchs J, Joshi RL, Moya KL, Prochiantz A (2018) The Physiology of Homeoprotein Transduction. *Physiol Rev* 98(4):1943–1982.
19. Esko JD, Stewart TE, Taylor WH (1985) Animal cell mutants defective in glycosaminoglycan biosynthesis. *Proc Natl Acad Sci U S A* 82(10):3197–3201.
20. Connor JP, Felder M, Kapur A, Onujiogu N (2012) DcR3 binds to ovarian cancer via heparan sulfate proteoglycans and modulates tumor cells response to platinum with corresponding alteration in the expression of BRCA1. *BMC Cancer* 12. doi:10.1186/1471-2407-12-176.
21. Vallen MJE, et al. (2014) Primary ovarian carcinomas and abdominal metastasis contain 4,6-disulfated chondroitin sulfate rich regions, which provide adhesive properties to tumour cells. *PLoS One* 9(11):1–10.
22. Maccarana M, Sakura Y, Tawada A, Yoshida K, Lindahl U (1996) Domain structure of heparan sulfates from bovine organs. *J Biol Chem* 271(30):17804–17810.
23. Turnbull JE, Gallagher JT (1991) Sequence analysis of heparan sulphate indicates defined location of N-sulphated glucosamine and iduronate 2-sulphate residues proximal to the protein-linkage region. *Biochem J* 277(2):297–303.
24. Lindahl U, Kusche-Gullberg M, Kjellen L (1998) Regulated diversity of heparan sulfate. *J Biol Chem* 273(39):24979–24982.
25. Burlina F, Sagan S, Bolbach G, Chassaing G (2005) Quantification of the cellular uptake of cell-penetrating peptides by MALDI-TOF mass spectrometry. *Angew Chemie - Int Ed* 44(27):4244–4247.
26. Burlina F, Sagan S, Bolbach G, Chassaing G (2006) A direct approach to quantification of the cellular uptake of cell-penetrating peptides using MALDI-TOF mass spectrometry. *Nat Protoc* 1(1):200–205.
27. Payne CK, Jones SA, Chen C, Zhuang X (2007) Internalization and trafficking of cell surface proteoglycans and proteoglycan-binding ligands. *Traffic* 8(4):389–401.
28. Belting M (2003) Heparan sulfate proteoglycan as a plasma membrane carrier. *Trends Biochem Sci* 28(3):145–151.
29. Häcker U, Nybakken K, Perrimon N (2005) Heparan sulphate proteoglycans: The sweet side of development. *Nat Rev Mol Cell Biol* 6(7):530–541.
30. Vannucchi S, Ruggiero M, Chiarugi V (1985) Complexing of heparin with phosphatidylcholine. A possible supramolecular assembly of plasma heparin. *Biochem J*

227(1):57–65.

31. Nyren-Erickson EK, et al. (2012) Glycosaminoglycan-mediated selective changes in the aggregation states, zeta potentials, and intrinsic stability of liposomes. *Langmuir* 28(46):16115–16125.
32. Alves ID, et al. (2008) Membrane interaction and perturbation mechanisms induced by two cationic cell penetrating peptides with distinct charge distribution. *Biochim Biophys Acta - Gen Subj* 1780(7–8):948–959.
33. Alves ID, et al. (2011) Relationships between membrane binding, affinity and cell internalization efficacy of a cell-penetrating peptide: Penetratin as a case study. *PLoS One* 6(9):e24096.
34. Bechtella L, et al. (2022) Structural Bases for the Involvement of Phosphatidylinositol-4,5-bisphosphate in the Internalization of the Cell-Penetrating Peptide Penetratin. *ACS Chem Biol* 17(6):1427–1439.
35. Tarbell JM, Cancel LM (2016) The glycocalyx and its significance in human medicine. *J Intern Med* 280(1):97–113.
36. Hauser H, Phillips MC, Levine BA, Williams RJP (1976) Conformation of the lecithin polar group in charged vesicles. *Nature* 261(5559):390–394.
37. Krumbiegel M, Arnold K (1990) Microelectrophoresis studies of the binding of glycosaminoglycans to phosphatidylcholine liposomes. *Chem Phys Lipids* 54(1):1–7.
38. Satoh A, Toida T, Yoshida K, Kojima K, Matsumoto I (2000) New role of glycosaminoglycans on the plasma membrane proposed by their interaction with phosphatidylcholine. *FEBS Lett* 477(3):249–252.
39. Szekeres GP, et al. (2021) The interaction of chondroitin sulfate with a lipid monolayer observed by using nonlinear vibrational spectroscopy. *Phys Chem Chem Phys* 23(23):13389–13395.
40. Huang WYC, Boxer SG, Ferrell JE (2024) Membrane localization accelerates association under conditions relevant to cellular signaling. *Proc Natl Acad Sci* 121(10). doi:10.1073/pnas.2319491121.
41. Illien F, et al. (2016) Quantitative fluorescence spectroscopy and flow cytometry analyses of cell-penetrating peptides internalization pathways: Optimization, pitfalls, comparison with mass spectrometry quantification. *Sci Rep* 6(November):1–13.
42. Jiao CY, et al. (2009) Translocation and endocytosis for cell-penetrating peptide internalization. *J Biol Chem* 2009 Dec 4;284(49):33957-65.

**Figure 1.** Sequence of the peptides used in this study. All peptides have a carboxamide moiety at the C-terminus and contain a biotin-Gly<sub>4</sub> tag at the N-terminus except the chimeric peptides GAG<sup>En</sup>-H3 and GAG<sup>Otx</sup>-H3 that contain a biotin-Gly<sub>5</sub> tag.



(b)

Peptide name	GAG-targeting	H3	Net charge (+,-)	Average charge per residue
H3		SQIKIWFQNKRAIKK	+6 (6+, 0-)	0.38
GAG <sup>En</sup>	RSRKPKKKNPNKEDKRPR		+8 (10+, 2-)	0.44
GAG <sup>En</sup> -H3	RSRKPKKKNPNKEDKRPR	SQIKIWFQNKRAIKK	+14 (16+, 2-)	0.41
GAG <sup>Otx</sup>	RKQRRERTTFTRAQL		+5 (6+, 1-)	0.33
GAG <sup>Otx</sup> -H3	RKQRRERTTFTRAQL	SQIKIWFQNKRAIKK	+11 (12+, 1-)	0.35

**Figure 2.** Quantity of (a) H3 and GAG-binding sequences and (b) chimeric peptides internalized in one million cells after 1 hour incubation with peptides (7  $\mu$ M) at 37°C, determined by MALDI-TOF MS (25, 26). The amounts were normalized relative to H3 internalization in K1 cells.

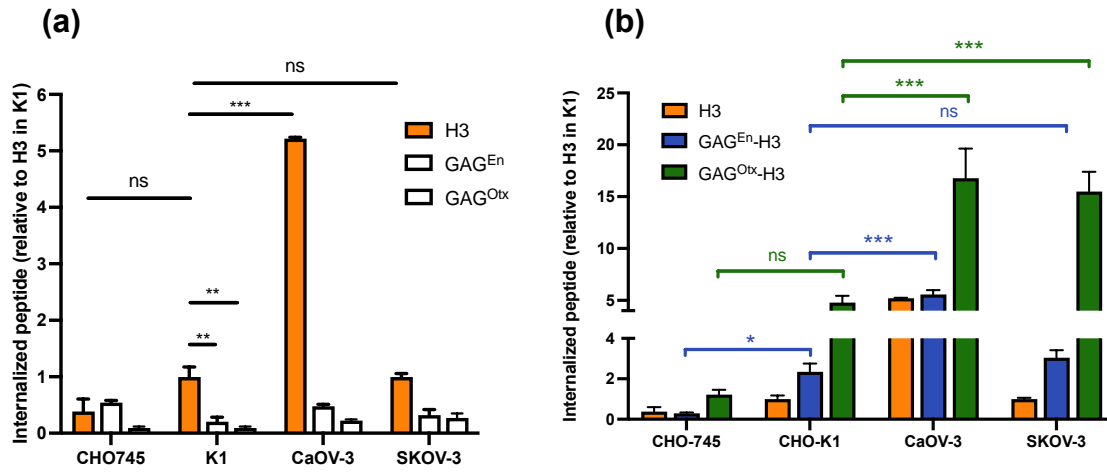


**Figure 3.** Quantity (pmoles) of internalized GAG<sup>En</sup>-linker-H3 and GAG<sup>Otx</sup>-linker-H3 analogues (the linker being either Apa, Pro, PEG<sub>2</sub>, Gly or Gly<sub>4</sub>), after incubation 37°C of 10 μM peptides with one million CHO-K1 cells, determined by MALDI-TOF MS.

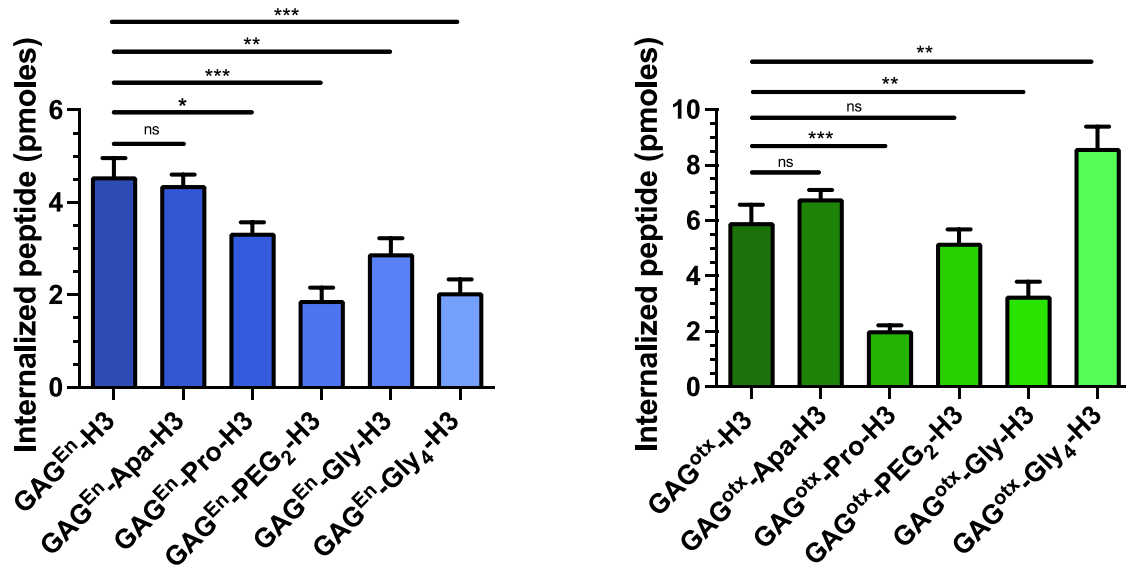
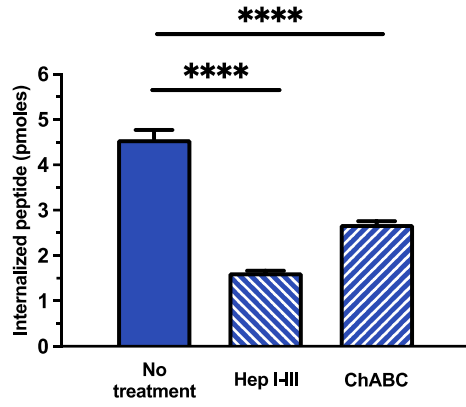


**Figure 4.** Effect of GAG degradation on the quantity (pmoles) of peptides internalized in one million SKOV-3 cells after 1 hour incubation with peptides (7  $\mu$ M) at 37°C, determined by MALDI-TOF MS.

**(a) GAG<sup>En</sup>-H3**



**(b) GAG<sup>Otx</sup>-H3**

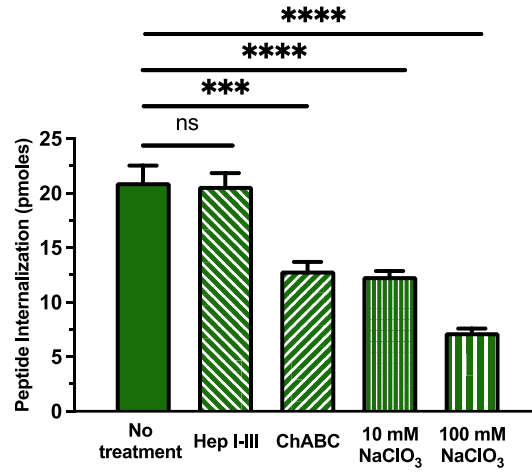


**Figure 5.** DSC analysis of  $T_m$  and enthalpy changes upon addition of heparin (HI) to 1 mg/ml DMPC LUVs in (a) HEPES buffer and (b) HEPES buffer plus  $\text{Ca}^{2+}$ ,  $\text{Mg}^{2+}$ . Curves correspond to DMPC mixed with different amounts of HI. The pre-transition of DMPC is circled by the dashed rectangle and zoomed in the left top; Corresponding main phase transition temperature (c) and enthalpy (d) of DMPC LUVs according to HI/DMPC ratio. The impact of  $\text{Ca}^{2+}$  on PC organization is schematically represented at the bottom : (a) in the absence of  $\text{Ca}^{2+}$ , the positively charged choline interacts with the negative phosphate moiety of the polar head, which creates steric hindrance or charge repulsion between the polar head groups of adjacent phospholipids; (b) in the presence of  $\text{Ca}^{2+}$ , the divalent ion bridges phosphate moieties, which allows the choline headgroup to reorientate outside the bilayer and induces lateral compression between adjacent alkyl chains.

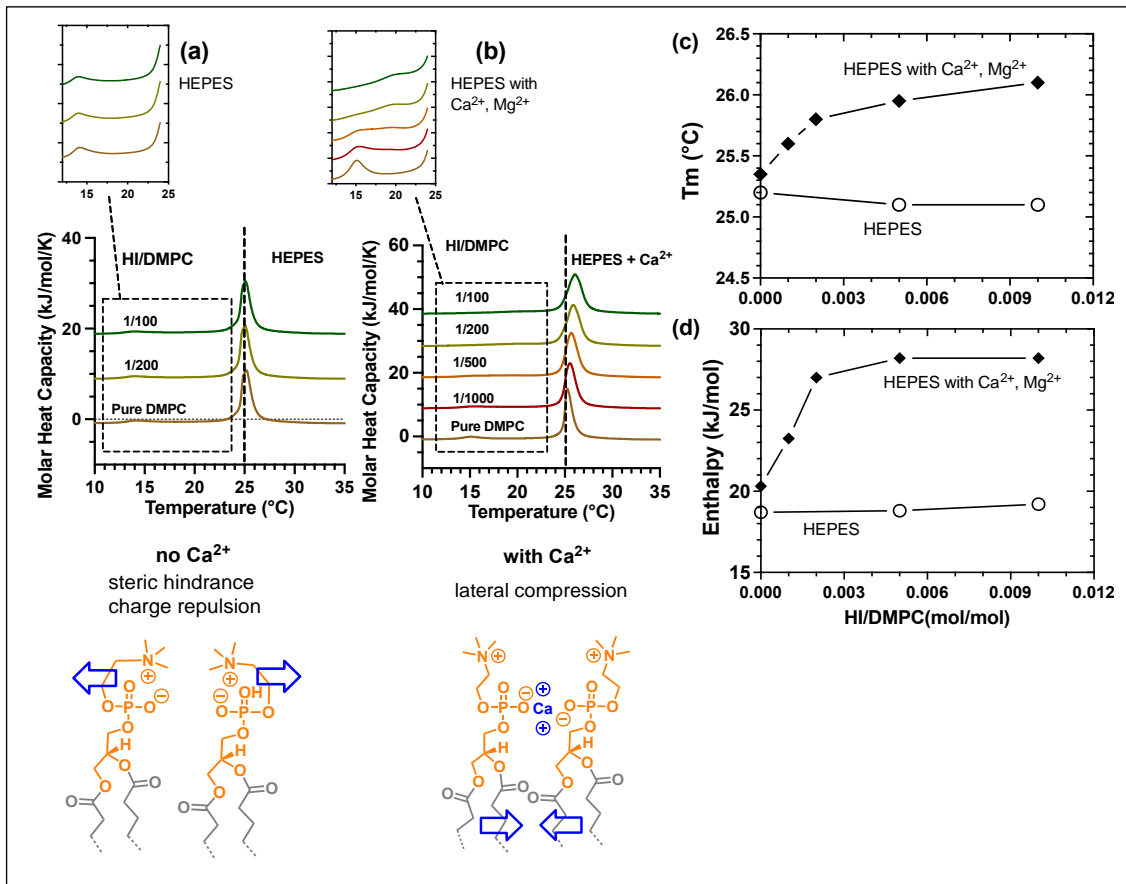


**Figure 6.** DSC analysis of enthalpy changes upon addition of GAG<sup>En</sup>-H3 (a, b, c) or GAG<sup>Otx</sup>-H3 (d, e, f) to 1 mg/mL HI- (grey) or CSE-decorated (pink) DMPC LUVs in HEPES buffer plus Ca<sup>2+</sup>, Mg<sup>2+</sup>. (c, f) Curves correspond to the relative  $\Delta H$  that is the ratio between the enthalpy recorded with GAG-decorated DMPC LUVs and the one with pure DMPC LUVs (blue), according to different ratios of peptide / DMPC LUVs.

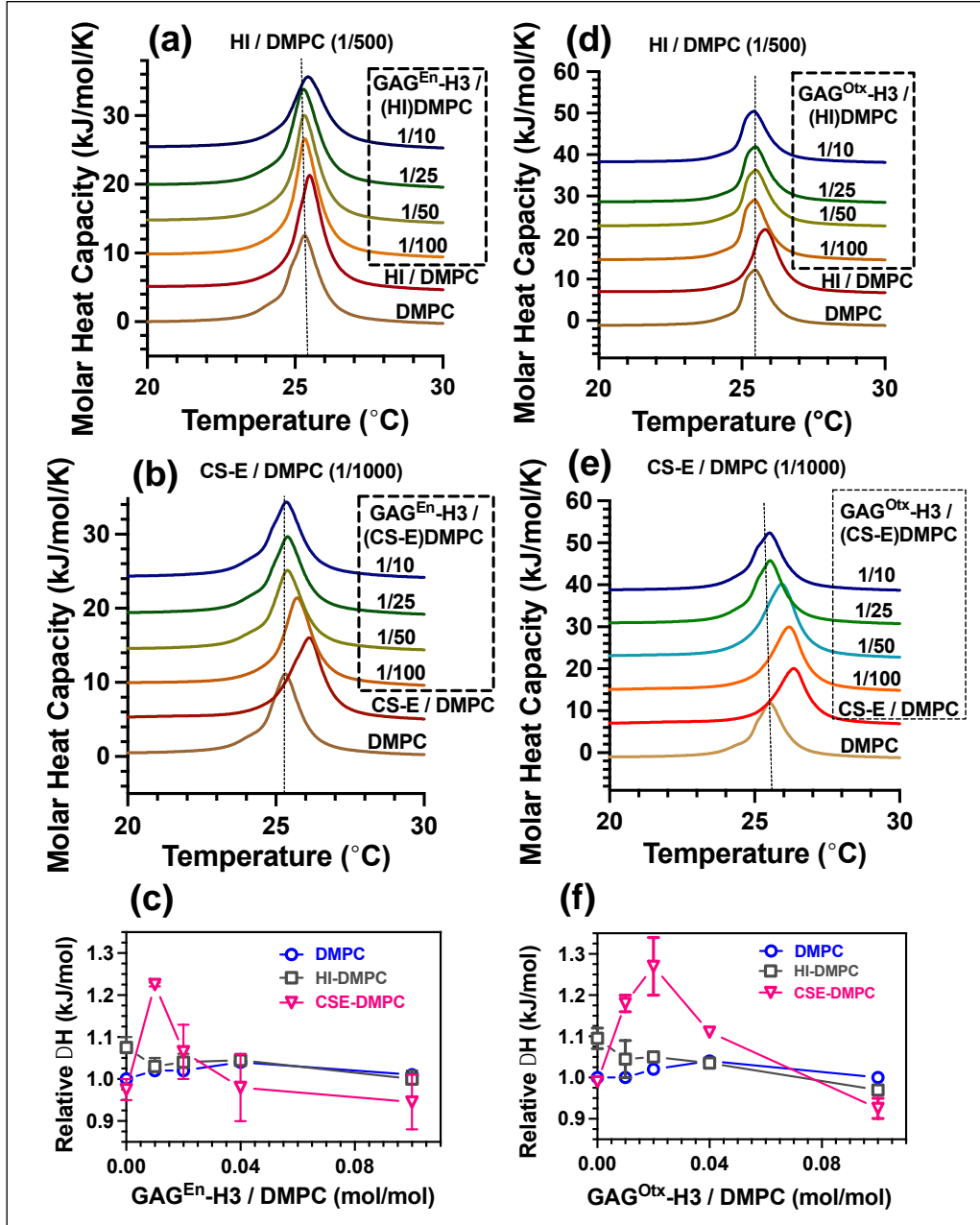


**Figure 7.** Mass spectrometry quantification of the internalization of 7  $\mu\text{M}$  GAG<sup>En</sup>-H3 or GAG<sup>Otx</sup>-H3 in pgsA-745 (a, b) or CaOV-3 (c, d) cells, in the absence or presence of various concentrations of HI (a, c) or CS-E (b, d). In panels (a, b), the quantity of internalized peptides is given in pmoles; in panel (c, d), the internalization of the peptide in the presence of HI or CS-E is given relatively (normalized), to the quantity measured in the absence of the exogenously added GAGs.

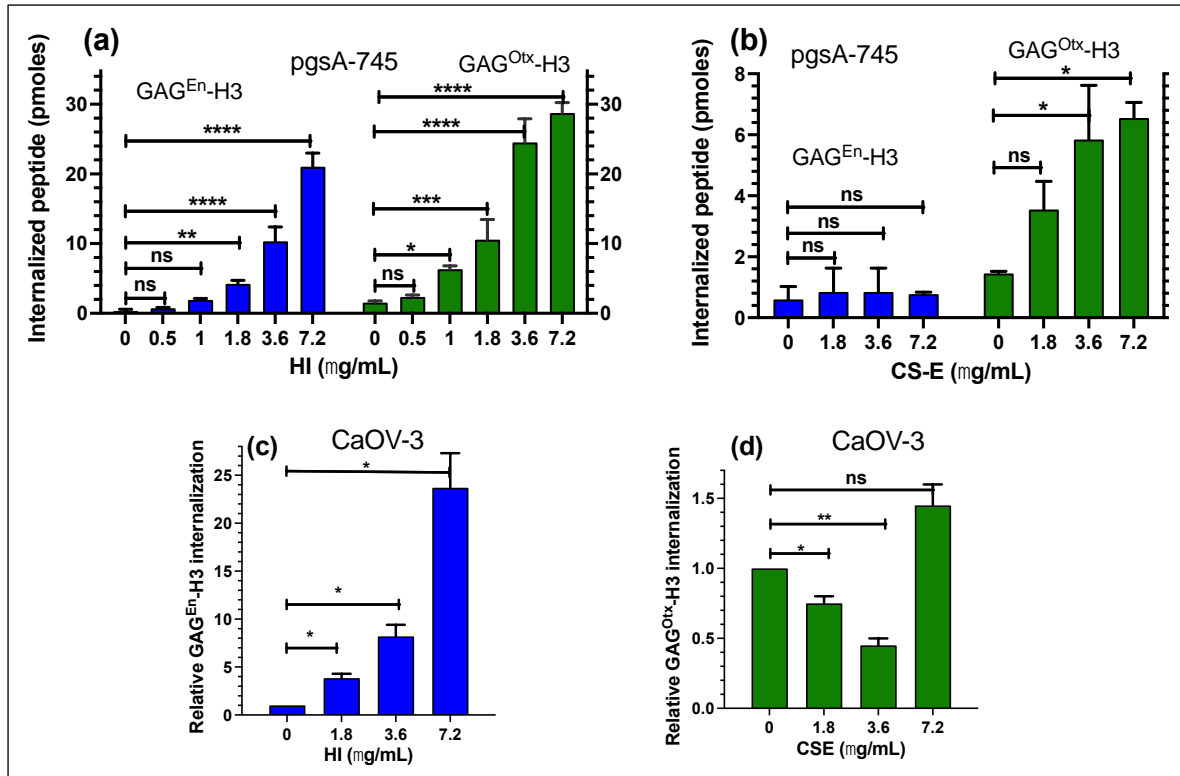


**Figure 8.** Schematic representation of the proposed role of GAGs in the internalization mechanism of the chimeric peptides studied herein. At low concentrations, chimeric cationic CPPs bind to HS- and CS- proteoglycans. (4S, 6S)-chondroitin sulfates bind PC lipids only in the presence of  $\text{Ca}^{2+}$ , leading to an overall zwitterionic complex. Therefore, there are no longer repulsion forces between the cationic choline headgroup and the cationic peptide, which can then insert deeper into the lipid bilayer to reach the cytosol. In parallel, the cationic peptides bind to HS- and CS-glycosaminoglycans but cannot evoke endocytosis that is activated at higher peptide concentrations. At high concentrations, the cationic peptides accumulate on HS- and CS-glycosaminoglycans and evoke endocytosis by clustering proteoglycans (42, 43).

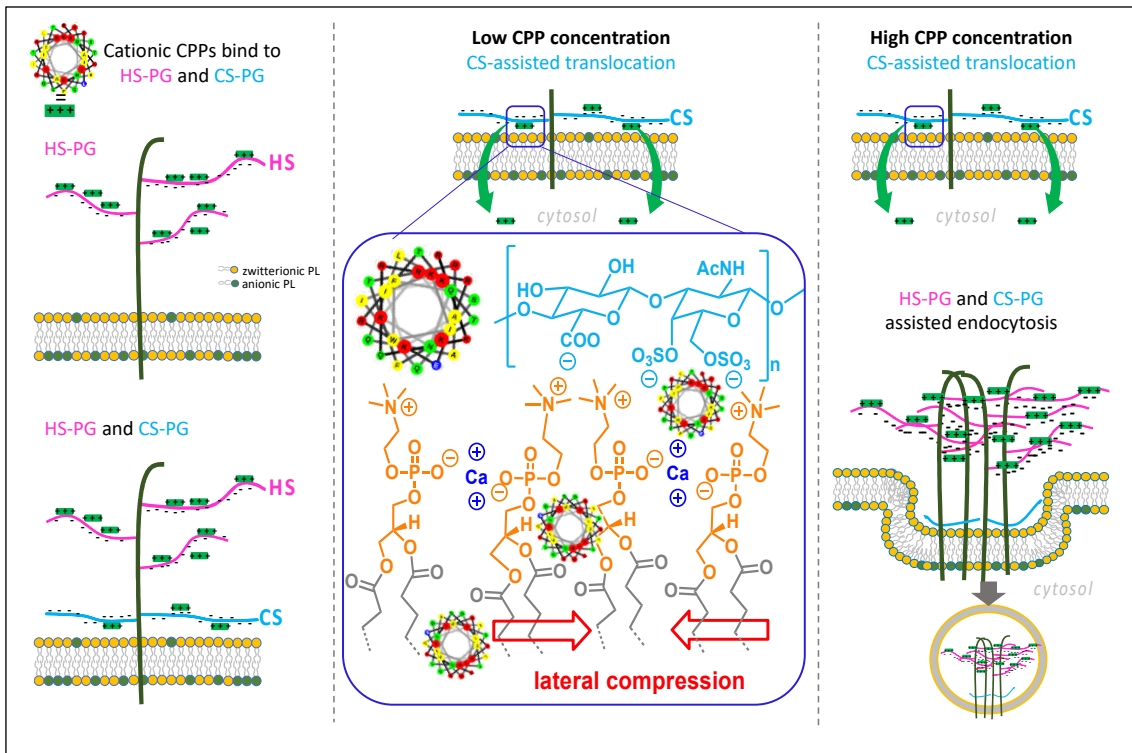


**Table 1.** ITC thermodynamics of peptides with 12 kDa heparin (HI) and 72 kDa (4S, 6S)-CS (CS-E). Peptides were titrated with the polysaccharides at 25°C in 50 mM NaH<sub>2</sub>PO<sub>4</sub> (pH 7.4), 100 mM NaCl. Results are shown as mean ± SD (n=3). To get access to the binding energy and dissociation constant of one peptide to one polysaccharide chain only, the global free energy of binding was divided by the number of peptides bound per polysaccharide, with the assumption or approximation that there is no cooperativity between peptides during their binding to the polyelectrolyte and that all binding sites are similar along the polymer. The dissociation constant was calculated as  $K_d = e^{-\Delta G/nRT}$ , where  $RT = 0.8314 \times 298 = 2.478 \text{ kJ.K}^{-1}.\text{mol}^{-1}$ .

Peptide (Net charge)	GAG	Stoichiometry (peptide/GAG)	Complex charge	$\Delta H$ (kJ/mol)	$-T\Delta S$ (kJ/mol)	$\Delta G/nRT$	Normalised Kd (mM)
H3 (+6)	HI	14 ± 0.1	84+/55-	-200 ± 14	+156 ± 14	-1.27	280
	CS-E	41 ± 3	246+/285-	-268 ± 53	+258 ± 40	-0.099	905
GAG <sup>En</sup> (+8)	HI	6.0 ± 0.4	48+/55-	-74 ± 4.0	+36 ± 4.0	-2.56	77
	CS-E	50 ± 20	400+/285-	-170 ± 30	+130 ± 9	-0.322	724
GAG <sup>otx</sup> (+5)	HI	17 ± 4.7	85+/55-	-28 ± 3.0	-8.0 ± 3.0	-0.854	425
	CS-E	100 ± 22	500+/285-	-60 ± 6	+11 ± 2.0	-0.198	820
GAG <sup>En</sup> -H3 (+8)	HI	4.5 ± 0.5	63+/55-	-108 ± 2.0	+66 ± 2.0	-3.766	23
	CS-E	25.5 ± 1.5	357+/285-	-291 ± 21	+249 ± 19	-0.665	514
GAG <sup>Otx</sup> -H3 (+8)	HI	11.5 ± 4.5	126+/55-	-163 ± 3.0	+117 ± 3.0	-1.61	199
	CS-E	70 ± 20	770+/285-	-746 ± 96	+693 ± 120	-0.305	736

**Table 2.** Dissociation constants of GAG<sup>En</sup>-H3 and GAG<sup>Otx</sup>-H3 obtained by Trp fluorescence spectroscopy for each peptide binding to HI- and CS-E-decorated DOPC LUVs in the presence of Ca<sup>2+</sup> and Mg<sup>2+</sup>, except when specifically mentioned. Values of ( $\Delta\lambda$ )<sub>max</sub> (nm) and K<sub>D</sub><sup>app</sup> (μM) were obtained from the fits of fluorescence data given in Figure S9. NA: not applicable.

		GAG <sup>En</sup> -H3		GAG <sup>Otx</sup> -H3		
		No lipids	+ DOPC	No lipids	+ DOPC	+ POPG
No GAG	( $\Delta\lambda$ ) <sub>max</sub> K <sub>D</sub> <sup>app</sup>	-	0 NA	-	0 NA	14 ± 0.5 0.21 ± 0.05
HI	( $\Delta\lambda$ ) <sub>max</sub> K <sub>D</sub> <sup>app</sup>	14 ± 5.3 5.3 ± 1.2	18 ± 1.2 6.1 ± 1.3	15 ± 1 3.3 ± 0.6	16 ± 0.5 3.3 ± 0.4	-
CS-E	( $\Delta\lambda$ ) <sub>max</sub> K <sub>D</sub> <sup>app</sup>	6 ± 0.5 0.25 ± 0.08	7 ± 0.5 0.44 ± 0.11	14 ± 1.1 0.5 ± 0.13	13 ± 0.6 0.13 ± 0.03	-
CS-E (no Ca <sup>2+</sup> )	( $\Delta\lambda$ ) <sub>max</sub> K <sub>D</sub> <sup>app</sup>	-	-	14 ± 0.5 0.39 ± 0.05	14 ± 1.2 0.49 ± 0.14	-

# Translocation of cell-penetrating peptides involving calcium-dependent interactions between anionic glycosaminoglycans and the phosphocholine bilayer

Bingwei He<sup>1</sup>, Sonia Khemaissa<sup>1</sup>, Sébastien Cardon<sup>1</sup>, Rodrigue Marquant<sup>1</sup>, Françoise Illien<sup>1</sup>, Delphine Ravault<sup>1</sup>, Fabienne Burlina<sup>1</sup>, Emmanuelle Sachon<sup>1,2</sup>, Astrid Walrant<sup>1</sup>, Sandrine Sagan<sup>1\*</sup>

Corresponding author: Sandrine Sagan, Sorbonne Université, Laboratoire des Biomolécules, CC182, 4 place Jussieu, 75005 Paris, France.

**Email:** sandrine.sagan@sorbonne-universite.fr

## **This file includes:**

Figures S1 to S11

Tables S1 and S2

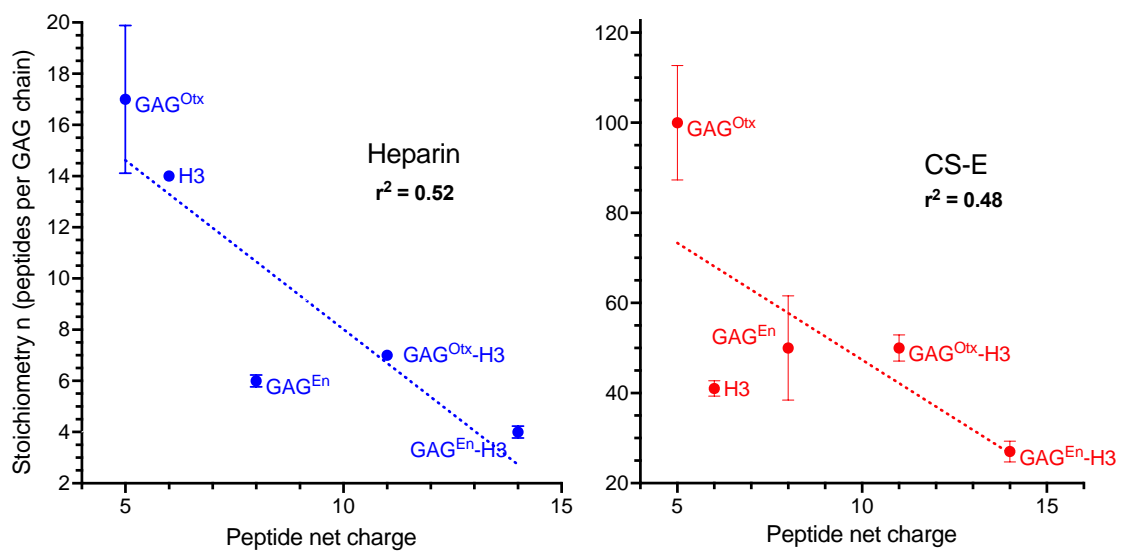


**Fig. S1.** Linear regression plot of the stoichiometry of GAG/peptide complexes (ITC) according to the net charge of the peptides: left panel, heparin (blue labels); right panel, CS-E (red labels).

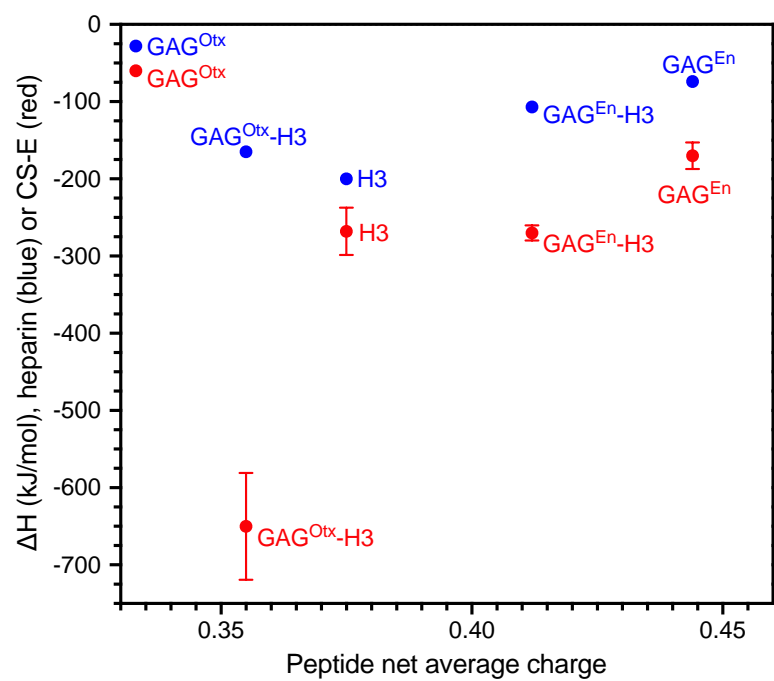


**Fig. S2.** Plot of enthalpy of formation of HI / peptide (blue labels), and CS-E / peptide (red labels), complexes according to the net average charge (net charge / number of AA), of the peptides.

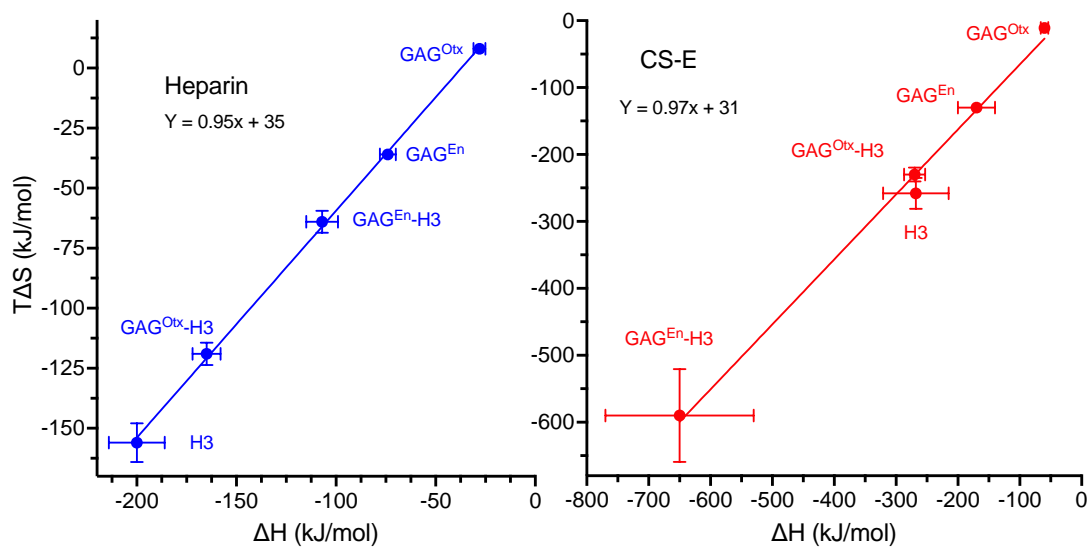


**Fig. S3.** Possible enthalpy-entropy compensation during formation of HI / peptide and CS-E / peptide complexes.

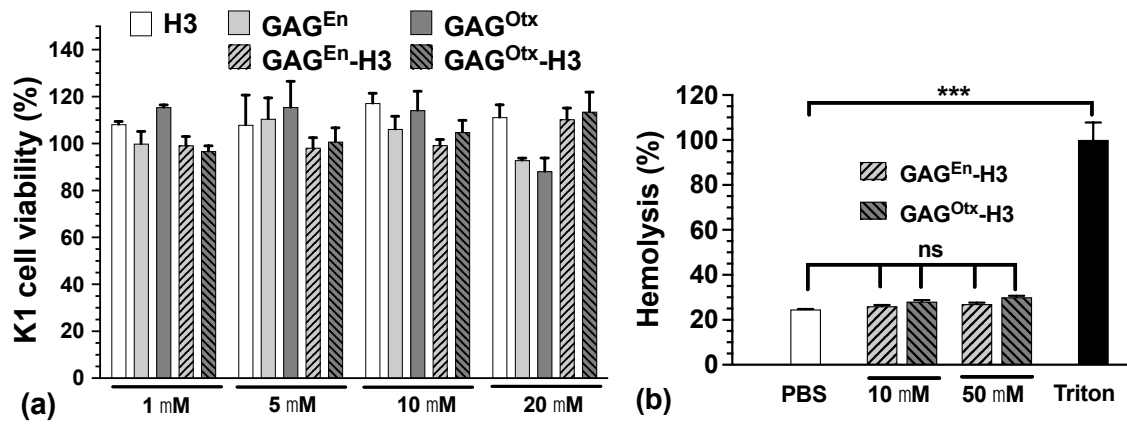


**Fig. S4.** Cytotoxicity of peptides incubated with CHO-K1 cells for 1 hr (a) and hemolysis of chimeric peptides after 2 hr incubation with blood cells (b) (\*\**p* < 0.001, highly significant; ns: not significant).

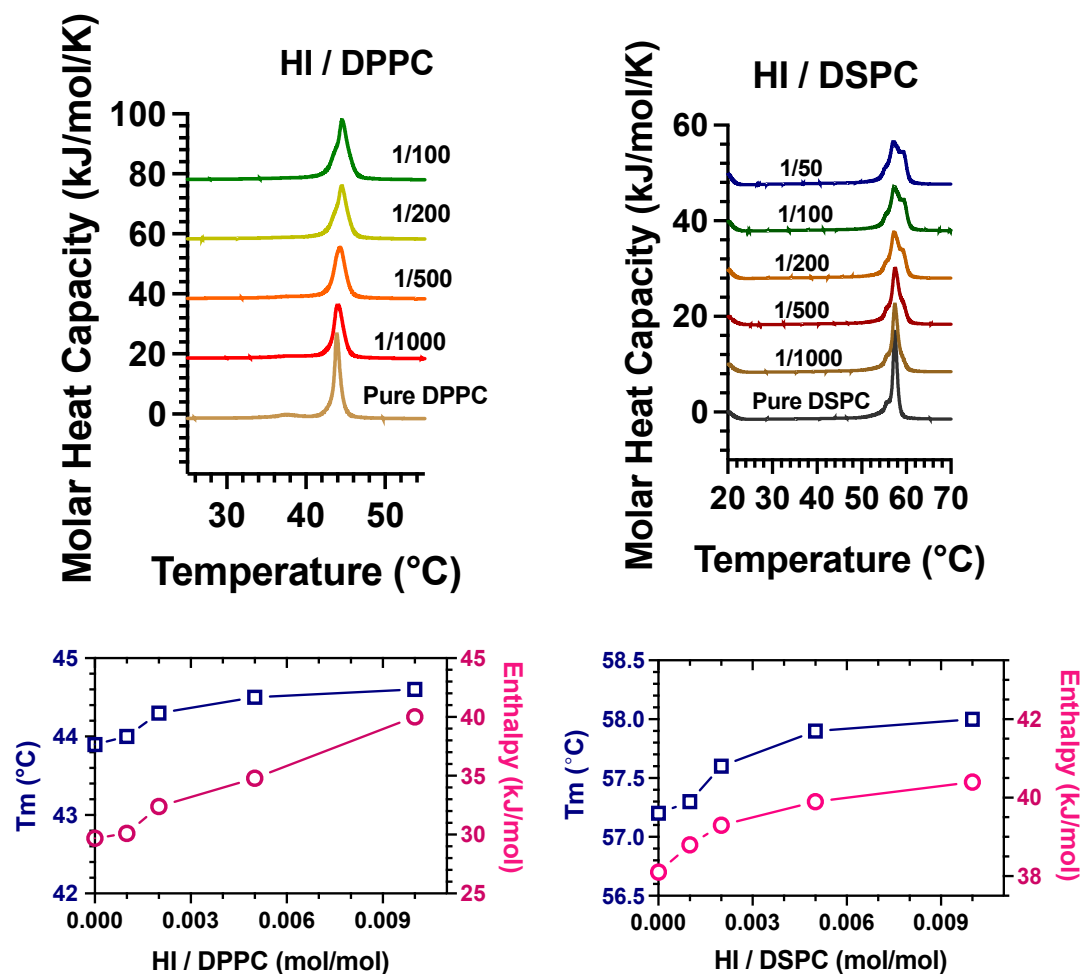


**Fig. S5.** DSC analysis of  $T_m$  and enthalpy changes upon addition of heparin (HI) to 1 mg/ml DPPC (left), or DSPC (right), LUVs in HEPES buffer plus  $Ca^{2+}$ ,  $Mg^{2+}$ . Curves correspond to LUVs mixed with different amounts of HI and show main phase transition temperature (blue), and enthalpy (pink), of LUVs according to HI/DMPDC ratio.

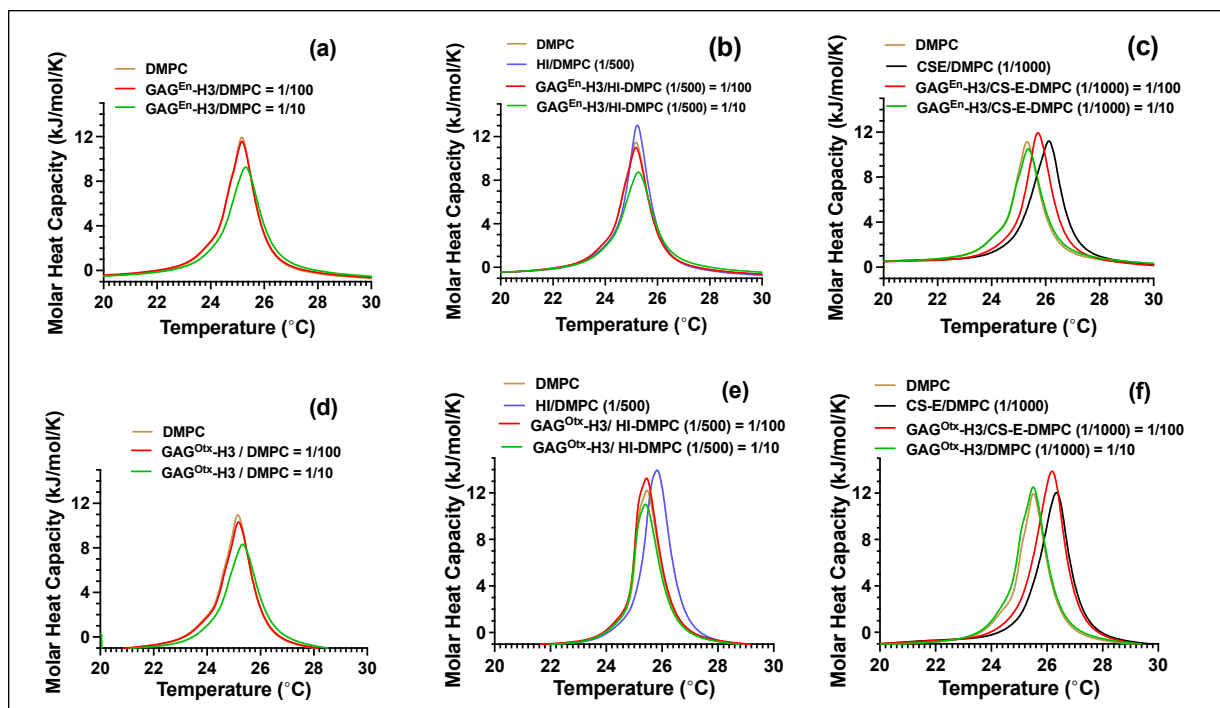


**Fig. S6.** DSC analysis of main transition  $T_m$  change of DMPC (1 mg/mL), upon addition of GAG<sup>En</sup>-H3 (a, b, c), or GAG<sup>Ox</sup>-H3 (d, e, f) in the absence (a, d) or the presence of heparin (HI with HI/DMPC ratio of 1/500, b, e), or CS-E (CS/DMPC ratio of 1/1000, c, f), in HEPES buffer plus Ca<sup>2+</sup>, Mg<sup>2+</sup>.

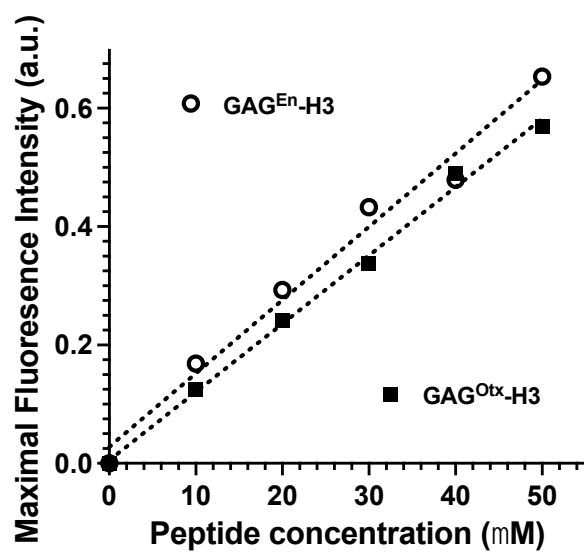


**Fig. S7.** Tryptophan fluorescence signal of increasing concentrations of GAG<sup>En</sup>-H3 (white circles), and GAG<sup>Otx</sup>-H3 (black squares).

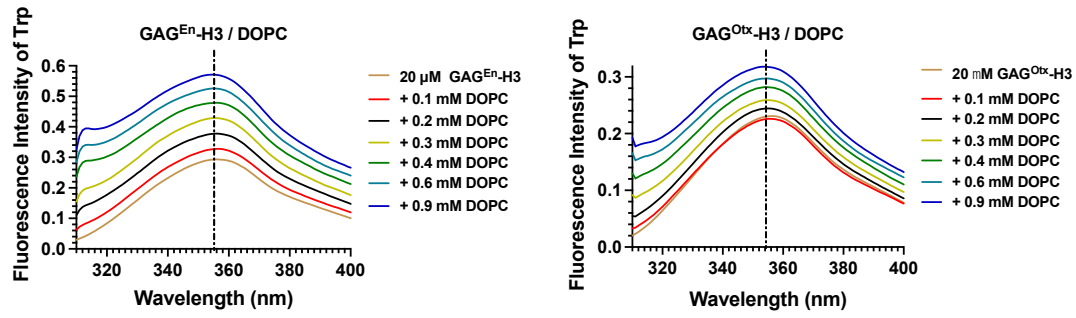


**Fig. S8.** Tryptophan fluorescence spectroscopy of GAG<sup>En</sup>-H3 (left), or GAG<sup>Otx</sup>-H3 (right) in the absence or the presence of increasing concentrations of DOPC LUVs, in HEPES buffer plus Ca<sup>2+</sup>, Mg<sup>2+</sup>. The dissociation constant K<sub>d</sub> (μM) is obtained for the 1/2 maximal wavelength shift,  $(\Delta\lambda_{\max})/2$ .

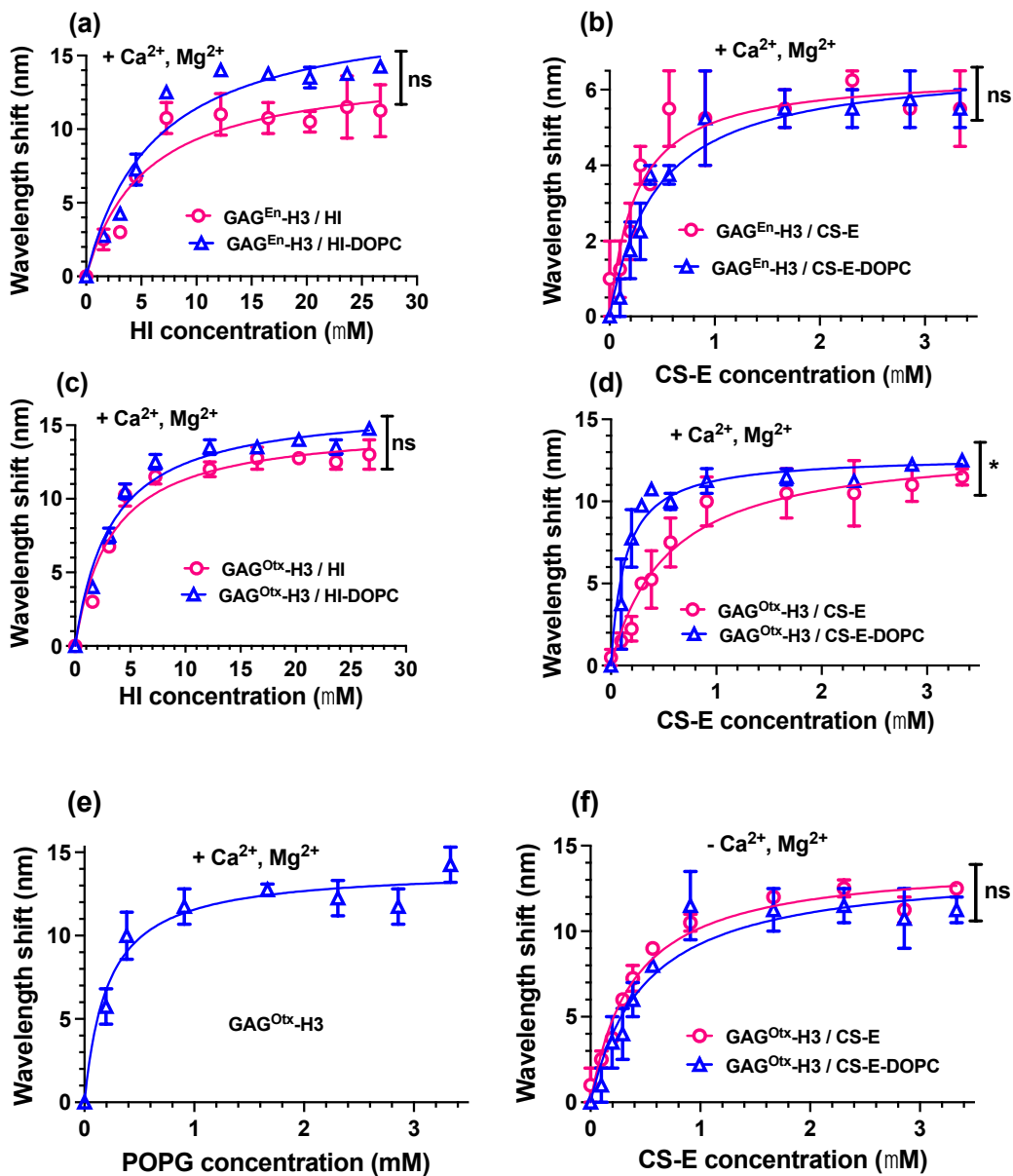


**Fig. S9.** Tryptophan fluorescence analysis of  $\text{GAG}^{\text{En}}\text{-H3}$  or  $\text{GAG}^{\text{Otx}}\text{-H3}$  binding to GAGs-decorated DOPC LUVs or POPG. Trp emission wavelength shift of  $\text{GAG}^{\text{En}}\text{-H3}$  binding to HI-DOPC vesicles (a), or CS-E-DOPC vesicles (b);  $\text{GAG}^{\text{Otx}}\text{-H3}$  binding to HI-DOPC vesicles (c), POPG vesicles (e), or CS-E-DOPC vesicles in the presence (d) or the absence of  $\text{Ca}^{2+}$  and  $\text{Mg}^{2+}$  (f).

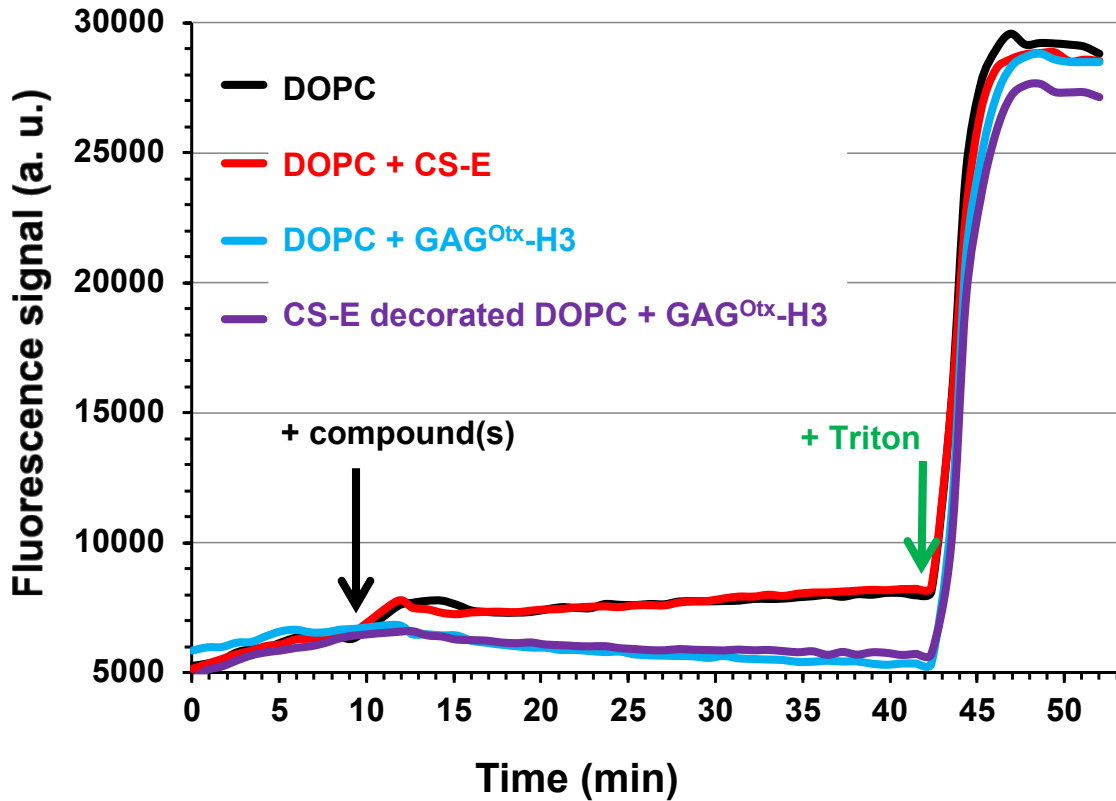


**Fig. S10.** Calcein leakage assay for measuring the potency of GAG<sup>Otx</sup>-H3 to damage the lipid bilayer, alone or in interaction with CS-E. The leakage of calcein from the DOPC or CS-E-decorated DOPC LUVs was monitored by measuring fluorescence intensity at an excitation wavelength of 485 nm and emission wavelength of 520 nm (FLUOstar OPTIMA, BMG Labtech). Determination of 100% dye-release was obtained with 10% Triton-X100 that dissolves the liposomes.

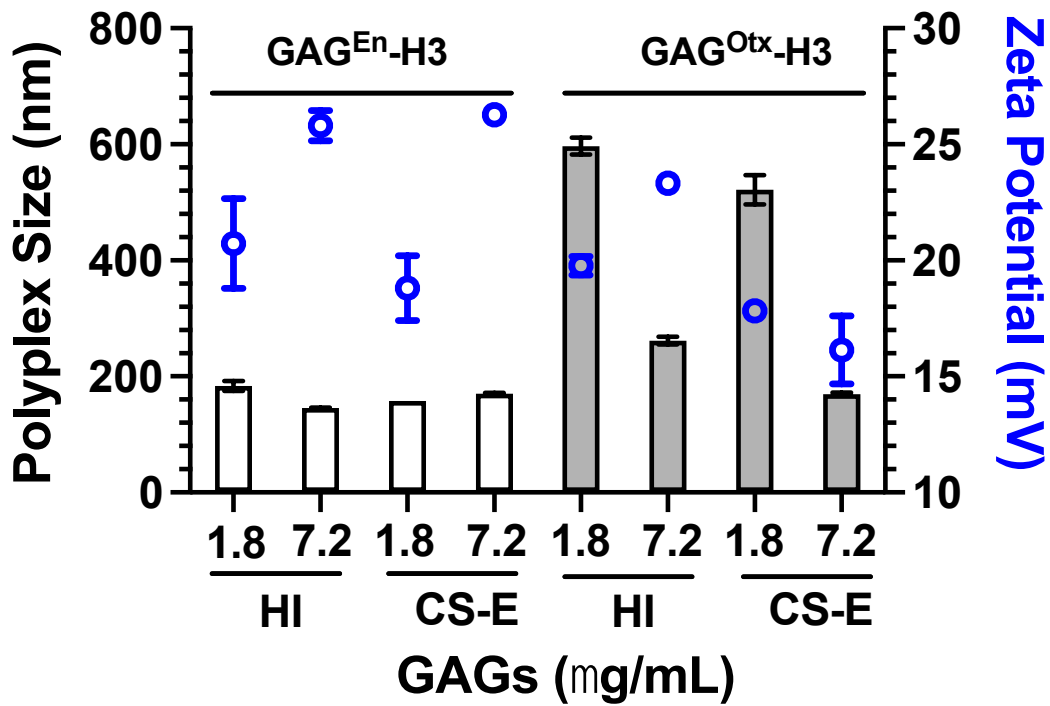


**Fig. S11.** Dynamic light scattering (DLS) and Zeta potential, giving the size (nm) and surface charge (mV), of association complexes between the peptide GAG<sup>En</sup>-H3 or GAG<sup>Otx</sup>-H3, and the GAG HI or CS-E.

**Table S1.** ITC thermodynamics of linker-containing peptides with 12 kDa heparin (HI) and 72 kDa (4S,6S)-CS (CS-E). Peptides were titrated with the polysaccharides at 25°C in 50 mM NaH<sub>2</sub>PO<sub>4</sub>, pH 7.4, 100 mM NaCl. Results are shown as mean ± SD (n=3). To get access to the binding energy and dissociation constant of one peptide to one polysaccharide chain only, the global free energy of binding was divided by the number of peptides bound per polysaccharide, with the assumption or approximation that there is no cooperativity between peptides during their binding to the polyelectrolyte and that all binding sites are similar along the polymer. The dissociation constant was calculated as  $K_d = e^{-\Delta G/nRT}$ , where  $RT = 0.8314 \times 298 = 2.478 \text{ kJ} \cdot \text{K}^{-1} \cdot \text{mol}^{-1}$ .

Peptide	polysacch. type	$\Delta G$ (kJ/mol)	$\Delta H$ (kJ/mol)	$-T\Delta S$ (kJ/mol)	stoich. n peptides per polysacch.	$\Delta G/nRT$	$K_d$ (mM) 1 peptide per polysacch.
<b>GAG<sup>60</sup>-H3</b>	HI	-42	-110 ± 2	68 ± 2	4.9 ± 0.7	-3.46	31
	CS-E	-44	-312 ± 24	268 ± 24	24 ± 1	-0.74	477
<b>GAG<sup>60</sup>-Apa-H3</b>	HI	-41	-126 ± 0	85 ± 1	5.6 ± 0.1	-2.95	52
	CS-E	-45	-448 ± 9	403 ± 9	29 ± 1	-0.63	534
<b>GAG<sup>60</sup>-Pro-H3</b>	HI	-42	-104 ± 1	62 ± 1	4.3 ± 0.1	-3.94	19
	CS-E	-133	-355 ± 26	222 ± 114	32 ± 5	-1.67	187
<b>GAG<sup>60</sup>-PEG-H3</b>	HI	-41	-104 ± 5	63 ± 4	4.9 ± 0.8	-3.37	34
	CS-E	-43	-317 ± 14	274 ± 14	27 ± 0	-0.64	526
<b>GAG<sup>60</sup>-Gly-H3</b>	HI	-41	-128 ± 2	87 ± 2	5.2 ± 0.5	-3.18	41
	CS-E	-44	-401 ± 15	357 ± 15	28 ± 1	-0.63	530
<b>GAG<sup>60</sup>-Gly<sub>4</sub>-H3</b>	HI	-43	-136 ± 7	93 ± 6	5.3 ± 0.6	-3.27	38
<b>GAG<sup>Otx</sup>-H3</b>	HI	-47	-161 ± 32	114 ± 33	16 ± 0.3	-1.19	306
	CS-E	-47	-843 ± 20	796 ± 20	91 ± 26	-0.21	812
<b>GAG<sup>Otx</sup>-APA-H3</b>	HI	-45	-145 ± 11	100 ± 10	11 ± 1	-1.65	192

	CS-E	-44	-688 ± 73	644 ± 73	63 ± 7	-0.28	1320
<b>GAG<sup>Otx</sup>-Pro-H3</b>	<b>HI</b>	<b>-43</b>	<b>-162 ± 9</b>	<b>119 ± 9</b>	<b>12 ± 3</b>	<b>-1.44</b>	<b>235</b>
	CS-E	-44	-672 ± 58	628 ± 59	65 ± 11	-0.27	761
<b>GAG<sup>Otx</sup>-PEG-H3</b>	<b>HI</b>	<b>-41</b>	<b>-146 ± 15</b>	<b>105 ± 15</b>	<b>22 ± 2</b>	<b>-0.75</b>	<b>471</b>
	CS-E	-44	742 ± 9	698 ± 10	67 ± 14	-0.27	767
<b>GAG<sup>Otx</sup>-Gly<sub>4</sub>-H3</b>	<b>HI</b>	<b>-45</b>	<b>-178 ± 4</b>	<b>133 ± 4</b>	<b>6 ± 0.4</b>	<b>-3.03</b>	<b>48</b>
	CS-E	-46	-780 ± 54	734 ± 54	40 ± 2	-0.46	629
<b>GAG<sup>Otx</sup>-Gly<sub>4</sub>-H3</b>	<b>HI</b>	<b>-40</b>	<b>-207 ± 5</b>	<b>167 ± 3</b>	<b>11 ± 1.0</b>	<b>-1.47</b>	<b>230</b>
	CS-E	-45	-878 ± 123	833 ± 122	67 ± 4	-0.27	763

**Table S2.** Circular dichroism analysis of chimeric peptide analogues incorporating different linkers, in phosphate buffer and 100 mM NaF, in interaction with heparin or POPG vesicles.

Phosphate buffer + 100 mM NaF													
Concentration	10 $\mu$ M						50 $\mu$ M						
Peptide	GAG <sup>Otx</sup> -H3						GAG <sup>Otx</sup> -H3						
Linker	None	Apa	Pro	PEG	Gly	4 Gly	None	Apa	Pro	PEG	Gly	4 Gly	
$\alpha$ Helix (%)	13	0	2	0	0	4	13	1	4	2	3	3	
Random coil (%)	71	66	73	69	70	87	79	77	81	83	79	84	
Type 2 Helix (%)	16	34	26	31	31	10	8	22	16	15	19	13	
$\beta$ strand (%)	0	0	0	0	0	0	0	0	0	0	0	0	
Phosphate buffer + 100 mM NaF + 2.3 $\mu$ M HI													
Concentration	10 $\mu$ M						50 $\mu$ M						
Peptide	GAG <sup>Otx</sup> -H3						GAG <sup>Otx</sup> -H3						
Linker	None	Apa	Pro	PEG	Gly	4 Gly	None	Apa	Pro	PEG	Gly	4 Gly	
$\alpha$ Helix (%)	0	0	1	4	0	6	13	5	7	4	5	4	
Random coil (%)	60	70	75	85	70	64	85	87	87	86	85	86	
Type 2 Helix (%)	0	0	0	0	0	1	2	9	5	11	10	9	
$\beta$ strand (%)	40	30	24	12	30	29	0	0	1	0	0	2	
Phosphate buffer + 100 mM NaF													
Concentration	10 $\mu$ M						50 $\mu$ M						
Peptide	GAG <sup>En</sup> -H3						GAG <sup>En</sup> -H3						
Linker	None	Apa	Pro	PEG	Gly	4 Gly	None	Apa	Pro	PEG	Gly	4 Gly	
$\alpha$ Helix (%)	0	0	0	0	0	0	0	0	0	0	0	0	
Random coil (%)	73	70	64	72	77	73	69	69	63	71	70	67	
Type 2 Helix (%)	27	30	36	28	23	27	31	31	37	29	30	33	
$\beta$ strand (%)	0	0	0	0	0	0	0	0	0	0	0	0	
Phosphate buffer + 100 mM NaF + 10 $\mu$ M HI													
Concentration	10 $\mu$ M						50 $\mu$ M						
Peptide	GAG <sup>En</sup> -H3						GAG <sup>En</sup> -H3						
Linker	None	Apa	Pro	PEG	Gly	4 Gly	None	Apa	Pro	PEG	Gly	4 Gly	
$\alpha$ Helix (%)	12	9	5	1	4	7	6	8	7	4	4	5	
Random coil (%)	70	71	52	51	69	62	88	89	87	83	83	87	
Type 2 Helix (%)	9	11	32	28	14	19	2	0	0	0	0	0	
$\beta$ strand (%)	9	9	12	20	12	13	4	3	7	13	14	8	
P/L = 1/50 (POPG)													
Peptide	GAG <sup>Otx</sup> -H3						GAG <sup>En</sup> -H3						
Spacer	None	Apa	Pro	PEG	Gly	4 Gly	None	Apa	Pro	PEG	Gly	4 Gly	
$\alpha$ helix (%)	60	37	44	36	59	36	0	0	1	1	1	1	
Random coil (%)	15	50	43	56	32	45	76	71	72	72	73	72	
Type 2 helix (%)	0	3	0	0	0	4	0	0	0	0	0	0	
$\beta$ strand (%)	25	10	13	9	9	16	27	28	27	27	26	27	
P/L = 1/25 (POPG)													
Peptide	GAG <sup>Otx</sup> -H3						GAG <sup>En</sup> -H3						
Spacer	None	Apa	Pro	PEG	Gly	4 Gly	None	Apa	Pro	PEG	Gly	4 Gly	
$\alpha$ helix (%)	30	10	20	6	12	0	nd	nd	nd	nd	nd	nd	
Random coil (%)	32	44	37	59	0	70	nd	nd	nd	nd	nd	nd	
Type 2 helix (%)	1	0	11	0	22	0	nd	nd	nd	nd	nd	nd	
$\beta$ strand (%)	37	46	32	35	66	30	nd	nd	nd	nd	nd	nd	
P/L = 1/10 (POPG)													
Peptide	GAG <sup>Otx</sup> -H3						GAG <sup>En</sup> -H3						
Spacer	None	Apa	Pro	PEG	Gly	4 Gly	None	Apa	Pro	PEG	Gly	4 Gly	
$\alpha$ helix (%)	0	0	0	3	2	2	nd	nd	nd	nd	nd	nd	
Random coil (%)	72	74	72	80	78	78	nd	nd	nd	nd	nd	nd	
Type 2 helix (%)	0	0	0	0	0	0	nd	nd	nd	nd	nd	nd	
$\beta$ strand (%)	28	25	28	17	20	20	nd	nd	nd	nd	nd	nd	